JCTC Journal of Chemical Theory and Computation

Article

pubs.acs.org/JCTC

Rational Design of Particle Mesh Ewald Compatible Lennard-Jones Parameters for +2 Metal Cations in Explicit Solvent

Pengfei Li, Benjamin P. Roberts, Dhruva K. Chakravorty, and Kenneth M. Merz, Jr.*

University of Florida, 2328 New Physics Building, PO Box 118435, University of Florida, Gainesville, Florida 32611-8435, United States

Supporting Information

ABSTRACT: Metal ions play significant roles in biological systems. Accurate molecular dynamics (MD) simulations on these systems require a validated set of parameters. Although there are more detailed ways to model metal ions, the nonbonded model, which employs a 12−6 Lennard-Jones (LJ) term plus an electrostatic potential, is still widely used in MD simulations today due to its simple form. However, LJ parameters have limited transferability due to different combining rules, various water models, and diverse simulation methods. Recently, simulations employing a Particle Mesh Ewald (PME) treatment for long-range electrostatics have become more and more popular owing to their speed and accuracy. In the present work, we have systematically designed LJ parameters for 24 +2 metal (M(II)) cations to reproduce different experimental properties appropriate for the Lorentz−Berthelot combining rules and PME simulations. We began by testing the transferability of currently available M(II) ion LJ parameters. The results showed that there are differences between simulations employing Ewald summation with other simulation methods and that it was necessary to design new parameters specific for PME based simulations. Employing the thermodynamic integration (TI) method and performing periodic boundary MD simulations employing PME, allowed for a systematic investigation of the LJ parameter space. Hydration free energies (HFEs), the ion−oxygen distance in the first solvation shell (IOD), and coordination numbers (CNs) were obtained for various combinations of the parameters of the LJ potential for four widely used water models (TIP3P, SPC/E, TIP4P, and TIP4P$_{EW}$). Results showed that the three simulated properties were highly correlated. Meanwhile, M(II) ions with the same parameters in different water models produce remarkably different HFEs but similar structural properties. It is difficult to reproduce various experimental values simultaneously because the nonbonded model underestimates the interaction between the metal ions and water molecules at short-range. Moreover, the extent of underestimation increases successively for the TIP3P, SPC/E, TIP4P$_{EW}$, and TIP4P water models. Nonetheless, we fitted a curve to describe the relationship between ε (the well depth) and radius ($R_{min}/2$) from experimental data on noble gases to facilitate the generation of the best possible compromise models. Hence, by targeting different experimental values, we developed three sets of parameters for M(II) cations for three different water models (TIP3P, SPC/E, and TIP4P$_{EW}$). These parameters we feel represent the best possible compromise that can be achieved using the nonbonded model for the ions in combination with simple water models. From a computational uncertainty analysis we estimate that the uncertainty in our computed HFEs is on the order of ±1 kcal/mol. Further improvements will require more advanced nonbonded models likely with inclusion of polarization.

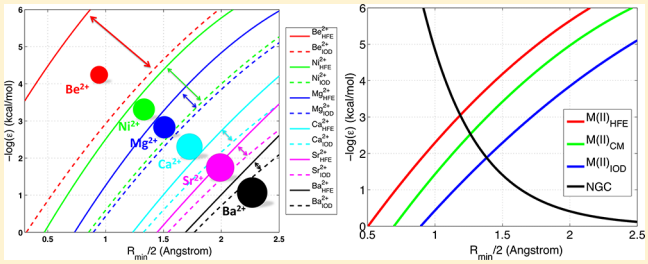

INTRODUCTION

Metal ions in biology carry out a myriad of important functions and are omnipresent in proteins.[1−4] More than 25 000 structures are returned when you use "metal" as a search keyword among the approximately 85 000 structures in the Protein Data Bank (PDB) database.[5] Metal ions such as calcium, zinc, iron, copper, manganese, nickel, and magnesium ions form complexes with surrounding amino acid residues and serve significant functional roles including structural, electron transfer, and catalytic functions.[1−4,6−15]

With the rapid development of supercomputers, the modeling of different enzyme systems has emerged as a rapidly growing field. Molecular dynamics (MD) simulation is a method based on Newtonian mechanics, which is widely used to investigate the dynamics and structural properties of protein systems. There are various modeling methods employed to describe metal ions in MD simulations including the bonded model,[5,16−21] the nonbonded model,[22,23] and the cationic dummy atom model.[24] The bonded model treats the metal ion and its ligating residues with bond, angle, and torsion terms together with point charges and van der Waals (VDW) terms, which is an accurate way to model the ions that form coordination bonds with surrounding residues. For instance, Peters et al. developed the MCPB (Metal Center Parameter Builder) software package,[5] which is used to facilitate the

Received: February 26, 2013
Published: May 8, 2013

ACS Publications © 2013 American Chemical Society

modeling of metal ions with a bonded plus electrostatics model in the AMBER force field (FF).[5] However, the coordination number (CN) remains fixed in the bonded model, and it is not designed to simulate ligand switching and CN changes. The nonbonded model treats the metal ion as a point with an integer charge, while the interactions are represented by Columbic and Lennard-Jones (LJ) terms. The coordination of the metal ion is flexible, which allows CN switching and ligand exchange at the metal center. However, this model oversimplifies the interaction between the ions and their surrounding residues. In addition to VDW and Columbic interactions, charge transfer, polarization, and even covalent interactions also exist between a metal ion and its surrounding ligands.[25−27] Furthermore, a single point poorly represents the charge distribution of most ions. It is usually nonsymmetrically distributed around the metal ion, which could also further change and redistribute in response to changes in the surrounding environment. The dummy cationic model is similar to the nonbonded model except it places charges between the metal ions and surrounding ligands to mimic the directionality of valence bonds.[24] Moreover, several other models, which employ functional forms somewhere between the bonded and nonbonded model, have also been developed in last two decades.[28−35] Meanwhile, several polarized FF models have been developed that incorporate charge transfer and polarization effects.[36−43]

Due to the simplicity of the nonbonded model, it is still extensively used for metal ions in MD simulations even though more sophisticated potential forms exist. In the nonbonded model, the only parameter one is required to determine is the appropriate LJ parameter. Åqvist designed LJ parameters for alkali and alkaline-earth metal cations with the hydration free energy (HFE) as a target property by performing free energy perturbation (FEP) simulations in 1990,[44] and these parameters have been adopted for use in early AMBER FFs. Merz developed Zn^{2+} LJ parameters by reproducing *ab intio* quantum mechanically calculated Zn^{2+}−CO_2 and Zn^{2+}−H_2O geometries and interaction energies.[45] Stote and Karplus characterized Zn^{2+} LJ parameters based on *ab initio* QM calculations fitting the Zn^{2+}−water potential energy surface as well as experimental data such as the Zn^{2+}−O first shell distance and absolute HFEs.[46] These parameters are now widely used in MD simulations. However, LJ parameters always have limited transferability between different water models, mixing rules and simulation conditions.[47−50] In recent years, Babu and Lim reoptimized LJ parameters for biologically relevant +2 metal (M(II)) cations based on experimental relative HFEs while the nonbonded interactions were truncated by an atom-based force switching function.[23] Joung and Cheatham developed a new set of LJ parameters for +1 metal ions specified for use with PME based MD simulations with target properties including experimental HFEs, the first peak of the radial distribution function (RDF), lattice energies and constants, as well as QM calculated ion−water interaction energies.[22] Recently, Allner et al. parametrized the LJ parameters for the Mg^{2+} ion based on the exchange rate.[51] Even so, there is a limited literature regarding LJ parameters designed specifically for M(II) ions in MD simulations employing the PME method, and this is the focus of the present work.

By employing the thermodynamic integration (TI) method,[52−59] we designed LJ parameters for 24 M(II) ions specifically for use in PME MD simulations. The present work contains four parts: (1) transferability testing of the LJ parameters in the extant literature, (2) quadratic fitting of experimental HFEs and the first peak of the ion−oxygen distance (IOD) based on the LJ parameter space for four popular water models (TIP3P,[60] SPC/E,[61] TIP4P,[60] and $TIP4P_{EW}$[62]), (3) final determination of the LJ parameters, and (4) assessment of these parameters. Based on our simulation results, we found that the transferability of existing LJ parameters for M(II) ions is limited. The four water models have different properties and should be treated separately when designing the parameters. The simulated HFE, IOD, and CN values are highly correlated, and there appears to be a one-to-one correspondence between them. Moreover, due to the simplicity of the nonbonded model, we could not reproduce all HFE, IOD, and CN values simultaneously. Based on different potential applications, we designed three separate sets of parameters for the TIP3P, SPC/E, and $TIP4P_{EW}$ water models: one for reproduction of experimental HFEs, one for experimental IOD values, and a final set representing a compromise between the former two properties (we term these the HFE, IOD, and CM sets, respectively). Overall, the HFE parameter set achieved an error range of ∼±1.0 kcal/mol for the absolute hydration free energy and ∼±2.0 kcal/mol for the relative free energy; the CM set achieved an error range of ±25.0 (or ∼6% of the total HFE) to ±40.0 (or ∼10% of the total HFE) kcal/mol (depending on the water model) for the absolute hydration free energy, ∼±2.0 kcal/mol for the relative free energy, and the IOD set achieved an accuracy of ∼±50.0 to ±75.0 kcal/mol (12% to 17% of total HFE, depending on the water model) for the absolute hydration free energy. All parameter sets showed generally good agreement with experimental IOD values with IOD being the best followed by CM and then the HFE parameter set. In the end, we evaluated the errors of the nonbonded model for different M(II) ions and found that TIP3P, SPC/E, $TIP4P_{EW}$, and TIP4P water models experience a successive increase in error. Furthermore, the stronger the coordination interaction between the M(II) metal ion and water molecules, in general, the larger the errors in the nonbonded model. This work marks a systematic investigation and determination of LJ parameters for various M(II) ions that can be employed in PME based MD simulations and these parameters are compatible with FFs such as AMBER and CHARMM when used with the PME model.

METHODS

Potential Function and Combining Rules. The potential function $U_{ij}(r_{ij})$ employed in the AMBER FF between nonbonded metal ions and other particles has the following form:

$$U_{ij}(r_{ij}) = \varepsilon_{ij}\left[\left(\frac{R_{\min,ij}}{r_{ij}}\right)^{12} - 2\left(\frac{R_{\min,ij}}{r_{ij}}\right)^{6}\right] + \frac{e^2 Q_i Q_j}{r_{ij}} \quad (1)$$

The first term is a 12−6 Lennard-Jones (LJ) potential while the second term is a classical Coulomb potential. In this formula, ε_{ij} is the well depth and $R_{\min,ij}$ represents the distance between two atoms at their lowest potential energy. r_{ij} is the distance between two atoms and e is the proton charge while Q_i and Q_j are the point charges for the two particles. In the AMBER FF, the VDW parameters follow the Lorentz−Berthelot combining rules as follows:

$$R_{\min,ij} = \frac{(R_{\min,ii} + R_{\min,jj})}{2} = R_{\min,i} + R_{\min,j} \quad (2)$$

$$\varepsilon_{ij} = \sqrt{\varepsilon_i \varepsilon_j} \quad (3)$$

The LJ parameters for the water models (TIP3P,[60] SPC/E,[61] TIP4P,[60] and TIP4P$_{EW}$[62]) employed in this work are shown in Table SI.1 in Supporting Information (SI).

Thermodynamic Integration. The free energy calculation of the hydration process employed the thermodynamic integration (TI) scaling method,[52−59] which has been shown to be an accurate method for calculating the free energy difference between two different states.[54] A mixing Hamiltonian $V(\lambda)$ between the initial and final states is used in the MD simulation as shown in eq 4. V_0 represents the initial state while V_1 represents the final state. λ represents the mixed thermodynamic state, $V(\lambda)$ is equal to V_0 when $\lambda = 0$ while $\lambda = 1$ results in $V(\lambda) = V_1$. k is an integer value and $k = 1$ results in linear mixing.

$$V(\lambda) = (1 - \lambda)^k V_0 + [1 - (1 - \lambda)^k] V_1 \quad (4)$$

For the linear soft-core scaling method[53] employed in this paper, $k = 1$ in eq 4 and a λ dependent modified LJ equation is employed (eq 5), where r_{ij} is the distance between the vanishing atom and the other atom, α is a constant set to 0.5, and σ equals $R_{\min,ij}/(2^{1/6})$. When $\lambda = 0$, it is identical to a normal form LJ equation, while when λ approaches 1, it displays a smooth interaction between the disappearing atom with its surrounding residues, allowing them to approach each other closely with a finite energy penalty.

$$V_{\text{soft-core VDW}} = 4\varepsilon(1 - \lambda)\left[\frac{1}{\left[\alpha\lambda + \left(\frac{r_{ij}}{\sigma}\right)^6\right]^2} - \frac{1}{\left[\alpha\lambda + \left(\frac{r_{ij}}{\sigma}\right)^6\right]}\right] \quad (5)$$

The derivative of the $\partial V/\partial\lambda$ is integrated to obtain the free energy difference in the constant pressure and temperature ensemble. The results could also be fit to a cubic spline or quadratic curve. In this work, we employed the Gaussian quadrature formula[55] (eq 8) to get the final free energy difference. Herein, we run a mixture of NVT and NPT simulations, so we make the approximation:

$$\Delta A = \Delta G \quad (6)$$

and

$$\Delta A = A(\lambda = 1) - A(\lambda = 0) = \int_0^1 \langle \partial V/\partial\lambda \rangle_\lambda \, d\lambda \quad (7)$$

$$\Delta A = \sum w_i \langle \partial V/\partial\lambda \rangle_i \quad (8)$$

In the present work, λ values were set to 0.1127, 0.5, and 0.88729 in a three-window TI simulation. λ values were chosen as 0, 0.1127, 0.5, 0.88729, and 1 for five-window scaling; λ values were 0, 0.04691, 0.23076, 0.5, 0.76923, 0.95308, and 1 for seven-window scaling, while for a nine-window TI simulation λ, values were set to 0, 0.2544, 0.12923, 0.29707, 0.5, 0.70292, 0.87076, 0.97455, and 1. Each window began from the final snapshot of the previous window, the windows of $\lambda = 0$ and 1 serve to equilibrate the system and are not considered in the final free energy calculation with eq 8.

Simulation Protocols. *Modeling and Initial Structure Preparation.* All simulations were carried out with the AMBER 11 suite of programs[63] while the modeling and data analyses were performed using the AmberTools suite of programs.[63] A schematic illustration of the work-flow is presented in Scheme SI.1. First, we created a ∼(46Å×46Å×46Å) cubic water box surrounding a dummy atom with the closest distance between any water molecule at 1.5 Å. In total, there were 2439 water molecules in the system for the TIP3P and SPC/E water models while for the TIP4P and TIP4P$_{EW}$ water models this number was 2389. We performed a minimization with 1000 steps of steepest descent minimization plus 1000 steps of conjugate gradient minimization. A 1 ns NVT heating procedure was followed to heat the system from 0 K to 300 K. A second 1 ns NVT at 300 K was performed to equilibrate the system. To ensure the correct system density, a 1 ns NPT simulation under 1 atm and 300 K conditions was performed, and the final structure was treated as the starting structure for TI simulations in the NPT ensemble in Method 2 (details below). Finally, another 1 ns NVT simulation was conducted to prepare the initial structure for TI simulations in the NVT ensemble for Method 1 (details below). For all simulations, periodic boundary condition (PBC) was employed together with PME to model long-range interactions. The time-step used is 1 fs with a 10 Å cut off. Test simulations performed by us (see Table SI.2) and others[22] indicated that the results were not sensitive to the choice of cutoff in the TI simulation under PME conditions. Langevin dynamics temperature control was employed with a collision rate equal to 5.0 ps^{-1}. SHAKE was utilized for the water molecules for all simulations.

For the determination of the HFE, we used the thermodynamic cycle shown in Figure 1. In the cycle HFE =

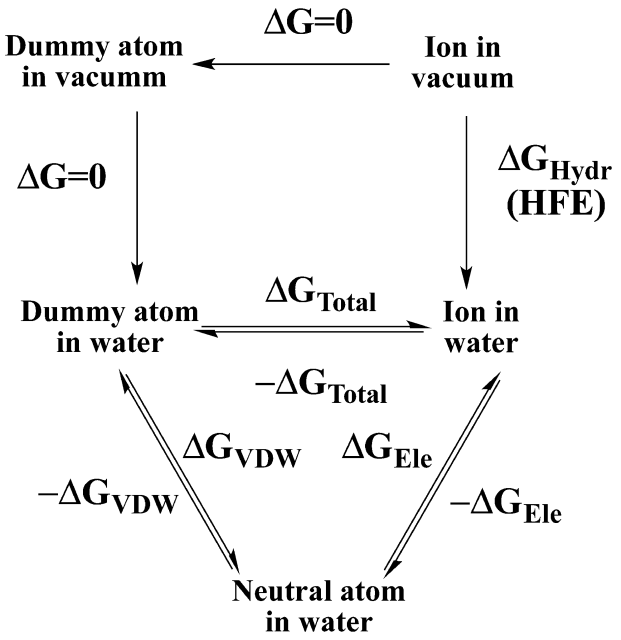

Figure 1. Thermodynamic cycle for calculating HFEs.

$\Delta G_{Total} = \Delta G_{VDW} + \Delta G_{Ele}$, where ΔG_{VDW} is the process by which the VDW term is turned on and ΔG_{Ele} involves turning on the Coulomb potential after turning on the VDW interaction, while ΔG_{Total} represents turning on the VDW and Coulomb potential simultaneously.

Scanning LJ Parameter Space. Overall, the simulations carried out consisted of two separate methods employing different simulation protocols. Method 1 was used to obtain

Table 1. Experimental HFE and IOD Values As Well As the First Solvation Shell CN Value for M(II) Metal Ions

ions	HFE (kcal/mol)[a]	relative HFE (M^{2+}-Cd^{2+}) (kcal/mol)	CN	IOD (Å)
Be^{2+}	−572.4	−152.9	4[b]	1.67[b]
Cu^{2+}	−480.4	−60.9	6[b]	Eq: 1.96 ± 0.04 Ax: 2.40 ± 0.10[b] weighted mean distance: 2.11[f]
Ni^{2+}	−473.2	−53.7	6[b]	2.06 ± 0.01[b]
Pt^{2+}	−468.5	−49.0	n	n
Zn^{2+}	−467.3	−47.8	6[b]	2.09 ± 0.06[b]
Co^{2+}	−457.7	−38.2	6[b]	2.10 ± 0.02[b]
Pd^{2+}	−456.5	−37.0	n	n
Ag^{2+}	−445.7	−26.2	n	n
Cr^{2+}	−442.2	−22.7	6[d]	Eq: 2.08[d]
Fe^{2+}	−439.8	−20.3	6[b]	2.11 ± 0.01[b]
Mg^{2+}	−437.4	−17.9	6[b]	2.09 ± 0.04[b]
V^{2+}	−436.2	−16.7	6[c]	2.21[c]
Mn^{2+}	−420.7	−1.2	6[b]	2.19 ± 0.01[b]
Hg^{2+}	−420.7	−1.2	6[b]	2.41[b]
Cd^{2+}	−419.5	0.0	6[b]	2.30 ± 0.02[b]
Yb^{2+}	−360.9	58.6	n	n
Ca^{2+}	−359.7	59.8	8[e]	2.46[e]
Sn^{2+}	−356.1	63.4	6[d]	Eq: 2.33−2.34[d] Ax: 2.38−2.90[d] weighted mean distance: 2.62[b]
Pb^{2+}	−340.6	78.9	n	n
Eu^{2+}	−331	88.5	n	n
Sr^{2+}	−329.8	89.7	8−15[d]	2.64 ± 0.04[b]
Sm^{2+}	−328.6	90.9	n	n
Ba^{2+}	−298.8	120.7	9[g]	2.83[g]
Ra^{2+}	−298.8	120.7	n	n

[a]All the experimental hydration free energies were obtained from ref 73. [b]From ref 74. [c]From ref 75. [d]From ref 76. [e]From ref 77. [f]Calculated by the authors from the experimental data. [g]From ref 78. [n]Either no experimental data were available or the data were deemed unreliable by Ohtaki and Radnai.[76]

HFE, IOD, and CN values for different combinations of the LJ parameters via scanning parameter space. In this protocol, we performed LJ parameter space scanning for the M(II) ion−water system with fixed mass 65.4 g/mol (the choice of mass has a limited influence on the simulated hydration free energy and radial distribution of the metal ion−water system). The range of $R_{min}/2$ was chosen from 0.3 Å to 2.5 Å with a 0.1 Å interval and ε was evenly distributed in the range of $10^{-6} - 1$ kcal/mol with a logarithmic scale (in total, there are 23 different $R_{min}/2$ values and 7 different ε values, forming $23 \times 7 = 161$ different combinations of LJ parameters for the M(II) ions). All combinations of the LJ parameters were investigated for each water model in the present work. To balance speed and accuracy, we used a one-step method (turn on the VDW and electrostatic interactions of the metal ion in one step) to obtain ΔG_{Total}. First, the hydration of the metal ion was simulated in the NVT ensemble using a nine-window TI simulation where each window had a 200 ps simulation time. The $dV/d\lambda$ values in the last 150 ps were collected and averaged. ΔG_{Total} values were obtained via Gaussian quadrature using eq 8. Subsequently, we performed a 1 ns MD simulation with snapshots collected every 1000 steps over the last 500 ps of simulation to obtain IOD and CNs for the metal ions. IOD values were obtained from a two iteration quadratic fitting of the radial distribution function: the first quadratic fitting was done for the data within ±0.1 Å of the peak of the first solvation shell, and in total, 21 points at 0.01 Å intervals were considered along the RDF. The second quadratic fitting was performed over the data within ±0.1 Å of the point, which was closest to the apex of the first fitting. The final IOD value was obtained from this final fit up to two decimal places. The CNs were determined via integrating the ion-oxygen RDF from the origin to the first minimum of the RDF. Finally, we carried out the reverse TI simulation to obtain $-\Delta G_{Total}$ with the same method used to obtain ΔG_{Total}. The $-\Delta G_{Total}$ and ΔG_{Total} values were then averaged in order to determine the HFE.

Final Parameter Determination. For our final determination of the LJ parameters, we employed Method 2, which is a more consistent method to obtain HFE, IOD, and CN values. Using TI simulations, we determined the ΔG_{VDW}, ΔG_{Ele}, $-\Delta G_{Ele}$, and $-\Delta G_{VDW}$ values (which correspond to the free energy changes for the VDW-appearing, charge-appearing, charge-disappearing and VDW-disappearing steps, respectively; see Figure 1) in the NPT ensemble consecutively. For ΔG_{VDW} and $-\Delta G_{VDW}$, we employed a three-window soft-core scaling method due to its better performance than both linear and nonlinear scaling methods.[53] For these steps, each window covered 300 ps and data were collected and averaged over the last 200 ps of simulation to obtain $dV/d\lambda$. The ΔG_{Ele} and $-\Delta G_{Ele}$ values were all obtained from a nine-window TI simulation of 200 ps where the last 150 ps were used for data collection. Finally, we obtained the HFE by averaging $\Delta G_{VDW} + \Delta G_{Ele}$ and $-(\Delta G_{VDW} + \Delta G_{Ele})$. For all TI simulations in the NPT ensemble, the anisotropic pressure scaling was performed with a 10 ps relaxation time and the same temperature control as TI scaling in the NVT ensemble. Finally, we modeled the metal ion−water system again, performed a 2000 step minimization (1000 steps of steepest descent plus 1000 steps of conjugate gradient), 500 ps NVT heating, 500 ps NPT equilibration, and a 2 ns NPT production run with snapshots

Table 2a. Absolute HFE, IOD, and CN Values of M(II) Ions Employing Parameters Available in the AMBER Package

	LJ param.		results from Method 2			results from Åqvist[44]	
	$R_{min}/2$(Å)	ϵ(kcal/mol)	HFE kcal/mol)	IOD (Å)	CN	HFE (kcal/mol)	IOD (Å)
Zn^{2+}	1.10	0.0125	−443.8	1.93	6.0		
Mg^{2+}	0.7926	0.8947	−432.6	1.99	6.0	−455.9 ± 2.6	2.00
Ca^{2+}	1.7131	0.459789	−307.0	2.70	8.9	−380.6 ± 1.3	2.40

Table 2b. Absolute HFE, IOD, and CN Values of Zn(II) Employing Parameters Developed by Stote and Karplus

	LJ param.		results from Method 2			results from Stote and Karplus[46]	
	$R_{min}/2$ (Å)	ϵ(kcal/mol)	HFE (kcal/mol)	IOD (Å)	CN	HFE (kcal/mol)	IOD (Å)
Zn^{2+}	1.094	0.250	−399.9	2.10	6.0	−472.7	2.12

Table 2c. Absolute HFEs, Relative HFEs (Relative to the Cd^{2+} Ion), IOD Values, and CNs of M(II) Ions with the Parameters Taken from Babu and Lim.[23]

	LJ param.		results from Method 2				results from Babu and Lim[23]		
Ions	$R_{min}/2$ (Å)	ϵ(kcal/mol)	HFE (kcal/mol)	Relative HFE (kcal/mol)	IOD (Å)	CN	Relative HFE (kcal/mol)	IOD (Å)	CN
Be^{2+}	0.5637	0.0032	−521.4	−145.7	1.45	3.3	−156.3	1.57	4
Cu^{2+}	1.033	0.0427	−436.5	−60.8	1.96	6.0	−59.9	1.94	6
Ni^{2+}	1.0941	0.0366	−430.3	−54.6	1.98	6.0	−53.2	1.97	6
Pt^{2+}	1.1376	0.0332	−425.6	−49.9	1.99	6.0	−48.3	1.97	6
Zn^{2+}	1.1489	0.0325	−423.7	−48.0	2.00	6.0	−47.5	2.00	6
Co^{2+}	1.2267	0.0286	−414.6	−38.9	2.03	6.0	−38.0	2.02	6
Pd^{2+}	1.236	0.0282	−413.3	−37.6	2.03	6.0	−37.3	2.02	6
Ag^{2+}	1.3107	0.0266	−403.1	−27.4	2.07	6.0	−26.6	2.06	6
Cr^{2+}	1.3344	0.0264	−399.2	−23.5	2.08	6.0	−22.4	2.07	6
Fe^{2+}	1.3488	0.0264	−397.0	−21.3	2.09	6.0	−20.5	2.08	6
Mg^{2+}	1.3636	0.0266	−394.4	−18.7	2.10	6.0	−17.5	2.08	6
V^{2+}	1.3706	0.0266	−393.5	−17.8	2.10	6.0	−16.2	2.11	6
Mn^{2+}	1.4544	0.03	−377.2	−1.5	2.17	6.1	−1.5	2.16	6
Cd^{2+}	1.46	0.0304	−375.7	0.0	2.18	6.1	0.0	2.17	6
Yb^{2+}	1.9298	0.0309	−317.2	58.5	2.57	8.3	57.7	2.47	8
Ca^{2+}	1.9364	0.0318	−316.7	59.0	2.58	8.3	58.1	2.58	8
Sn^{2+}	1.954	0.0346	−313.2	62.5	2.61	8.5	62.6	2.58	8
Pb^{2+}	2.0195	0.0557	−298.2	77.5	2.71	8.9	78.2	2.68	8.5
Eu^{2+}	2.0846	0.0647	−288.7	87.0	2.78	9.0	88.8	2.74	9
Sr^{2+}	2.0923	0.0664	−287.8	87.9	2.79	9.0	89.3	2.75	9
Sm^{2+}	2.0997	0.068	−286.5	89.2	2.79	9.0	90.1	2.75	9
Ba^{2+}	2.2451	0.1993	−257.8	117.9	3.04	9.8	120.4	3.01	9.5

stored after every 1000 steps for IOD and CN calculation by employing the same analysis method as Method 1. The comparison of each step's results with different cut off values is shown in Table SI.2, from which we can see (not surprisingly) there is no remarkable influence on the results for cut off values in the range of 8 to 12 Å when using the PME method.

To estimate computed uncertainties, two different methods were used and the results are given in the Supporting Information (SI) (note: the computed uncertainty tables correspond with the data tables given in the text) as Error Analysis Set 1 and Set 2. Note that the Tables (Table 9a, b and c) given in the text indicate error with respect to experimental values, while the computed uncertainties given in the SI correspond to uncertainties present in the computations themselves. For Method 1, the Set 1 computational uncertainty analysis was done by dividing the forward 150 ps and backward 150 ps of sampling into two 75 ps segments and calculating the HFEs separately and then finally obtaining the standard deviation using the resultant four values. For Method 2, the computational uncertainty of the charge and VDW components were obtained independently and the uncertainty in the computed HFE is the sum of them. The VDW scaling runs covered 200 ps forward and 200 ps backwards with each broken down into two 100 ps segments (4 segments total) for the uncertainty analysis. For the charge scaling runs the forward 150 ps and backward 150 ps were also broken down into two 75 ps segments for each (again 4 segments total) to do the uncertainty analysis.

Set 2 of the uncertainty data was obtained from the following equation:[64]

$$\delta A = \sqrt{\langle A^2 \rangle_c} \times \sqrt{2\tau_A/T} \tag{9}$$

where τ_A is the autocorrelation time of observable A, $(\langle A^2 \rangle_c)^{1/2}$ is the standard deviation of the observable A, T is the sampling time, and δA is the standard deviation σ of the final result. All of the final results were reported as $\langle A \rangle \pm 1\sigma$. Here, we use 250 fs for Method 1 and for the charge scaling part of Method 2. While for the VDW scaling part in Method 2, the correlation time was 500 fs. These two values came from several random test simulations we carried out and are also consistent with similar analyses performed by Shirts et al.[64] We can see from

the data provided in the SI that the values of the Set 1 HFE uncertainties range 0.1−3.5 kcal/mol (with an average of ∼0.6 kcal/mol), while the Set 2 values varied to a lesser extent (0.7−1.0 kcal/mol for an average of 0.9 kcal/mol)). Nonetheless, *in toto* these computational uncertainty analyses yielded similar average computational uncertainties for the computed HFEs. Hence, our best estimate of the computational uncertainty in our computed values is on the order of ±1 kcal/mol.

RESULTS AND DISCUSSION

Validation Tests of Several Available LJ Parameters for M(II) Ions. Experimental HFE, IOD, and CN values for 24 M(II) ions are given in Table 1. The general philosophy of parameter design is to make the best compromise estimate for

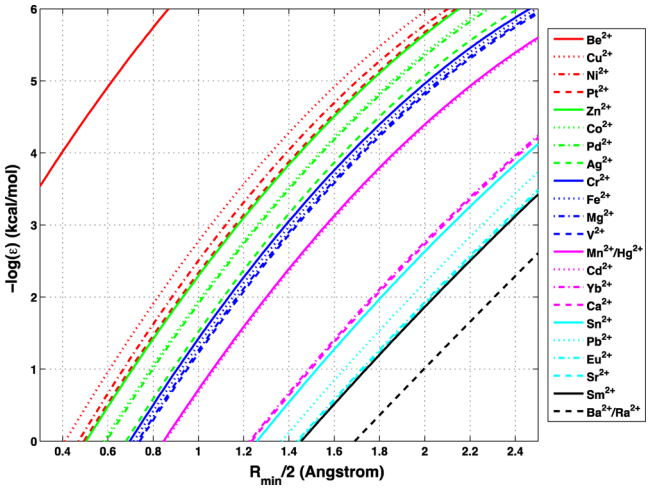

Figure 2. HFE fitting curves for 24 M(II) metal ions for the TIP3P water model.

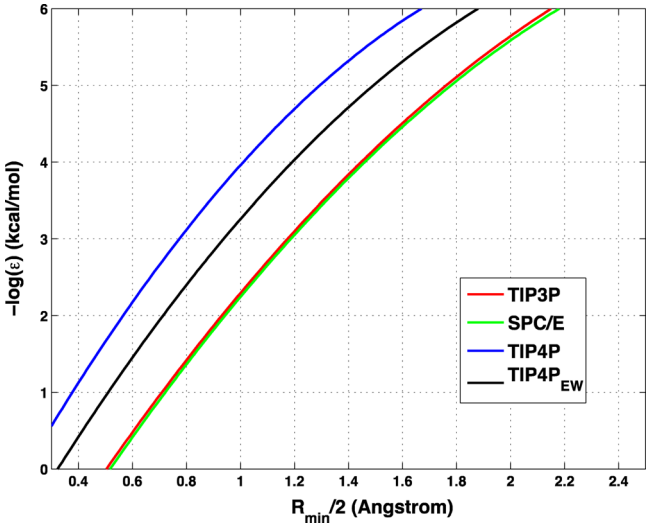

Figure 3. HFE fitting curves for Zn^{2+} in four different water models.

Table 3. Standard Deviation of the IOD Values for the LJ Grids (Å)

	TIP3P	SPC/E	TIP4P	$TIP4P_{EW}$
TIP3P	0.00	0.00 ± 0.01	0.02 ± 0.01	0.02 ± 0.01
SPC/E		0.00	0.02 ± 0.02	0.02 ± 0.01
TIP4P			0.00	0.00 ± 0.01
$TIP4P_{EW}$				0.00

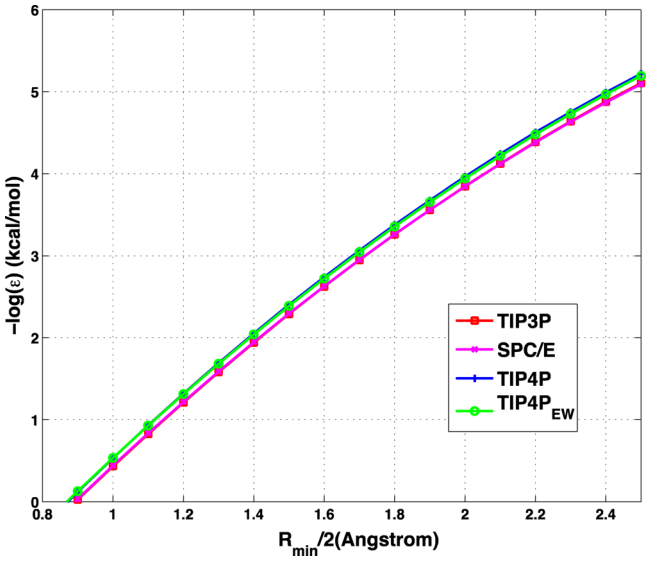

Figure 4. IOD fitting curves for Zn^{2+} in four different water models.

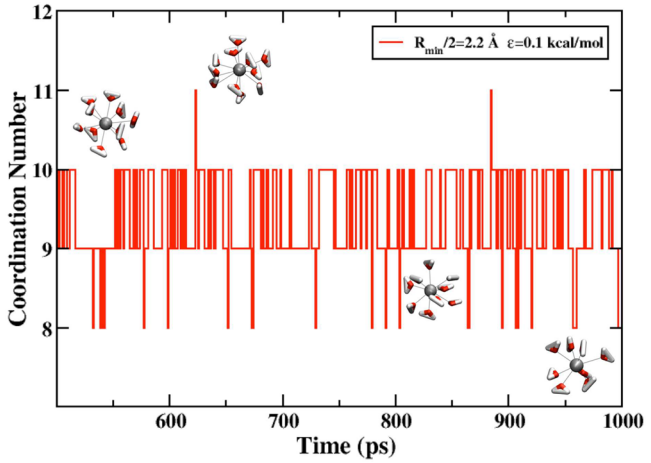

Figure 5. CN switching during a MD simulation when $R_{min}/2$ = 2.2 Å and ε = 0.1 kcal/mol with the TIP3P water model.

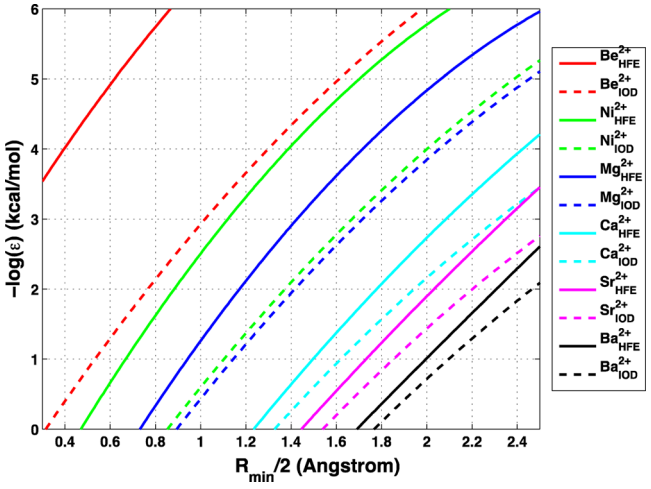

Figure 6. HFE and IOD fitting curves of six representative M(II) metal ions using TIP3P water model.

dx.doi.org/10.1021/ct400146w | J. Chem. Theory Comput. 2013, 9, 2733−2748

Table 4. LJ Parameters for Noble Gas Atoms[a]

	R_{min}(Å)	ε (meV)	$R_{min}/2$ (Å)	ε (kcal/mol)[b]	$-\log(\varepsilon)$(kcal/mol)
He	2.97	0.92	1.485	0.02121603	1.67333588
Ne	3.10	3.6	1.55	0.08301924	1.08082125
Ar	3.76	12.2	1.88	0.28134298	0.55076392
Ke	4.00	17.2	2.00	0.39664748	0.40159530
Ar	4.40	24	2.20	0.55346160	0.25691251

[a]Adapted from page 408 of Radètisig et al.[81] [b]Using the conversion factor 1 eV = 23.0609 kcal/mol.

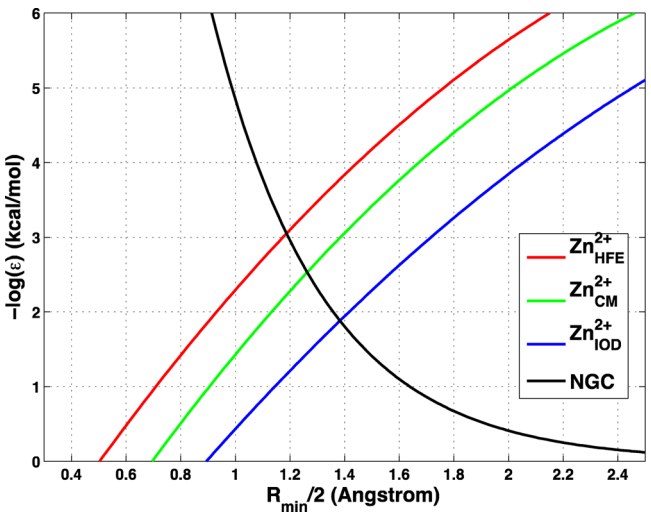

Figure 7. Determination of the three parameter sets for the Zn^{2+} ion in TIP3P.

different physical properties at the same time. In the first part of our work, we tested the transferability of LJ parameters, using the PME model and Method 2, for the M(II) ion parameter sets currently available in the AMBER FF parameter files.[44,45] The data from these simulations are shown in Table 2: Table 2a for the LJ parameters for Mg^{2+}, Ca^{2+}, and Zn^{2+} found in the AMBER parm99 FF, which is provided in the Amber Package.[63] In this FF, the Mg^{2+} and Ca^{2+} LJ parameters were adopted from Åqvist[44] by utilizing the Lorentz−Berthelot combining rules, while the Zn^{2+} LJ parameters were obtained from Merz.[45] Table 2b shows Zn^{2+} LJ parameters designed by Stote and Karplus[46] while Table 2c contains LJ parameters designed by Babu and Lim.[23] These results suggest that the differences between treating the long-range electrostatics with PME versus other methods cannot be simply overlooked. For example, Ca^{2+} in Table 2a has a large difference in the HFE and IOD values between the method employed in Åqvist's earlier work[44] and the PME method used in this work. The parameters in Table 2b did not have big differences (0.02 Å) in the IOD value, but it had significant differences in the simulated HFEs (~70 kcal/mol). The values in Table 2c indicate that Babu and Lim's parameters are shifted by ~45 kcal/mol from the experimental absolute HFEs, while they show good agreement with the PME simulations with respect to reproducing the relative HFEs. However, some metal ions still have notable differences (for example, Be^{2+} has a 10 kcal/mol difference in the relative HFE and 0.12 Å difference for the IOD between the two different methods). Based on the results shown, we decided that it was necessary to design a set of parameters for the M(II) metal ions using state-of-the art PME based MD simulations.

It is extremely important to note that we are not condemning the earlier efforts, all of which were excellent.[44−46] It simply reflects the fact that simulation protocols have evolved to the point where PME is the accepted standard for the treatment of long-range interactions, and it is possible to carry out very long MD simulations using this model with, for example, GPU technology.[65−72]

HFE and IOD Fitting Curves for Different Water Models. We cannot design a satisfactory unified M(II) ion parameter set for all popular water models since the parameter sets are different for the respective water models, which were shown in Table SI.1 in the SI. Hence, we performed simulations for different combinations of the $R_{min}/2$ and ε values for the TIP3P, SPC/E, TIP4P, and TIP4P$_{EW}$ water models, respectively. The HFE, IOD, and CN data obtained from Method 1 for each combination of LJ parameters with these water models are shown in Tables SI.3, and SI.4 in the SI. Based on the data shown in Table SI.3a (HFEs for TIP3P LJ grids), quadratic fitting was done for all of the 24 M(II) metal ions for the TIP3P water model, and the fitting curves are depicted in Figure 2. The fitting procedures are discussed in the SI, and the HFE fitting curves for all 24 M(II) metal ions for the SPC/E, TIP4P and TIP4P$_{EW}$ water models are given in Figure SI.1.

Figure 2 indicates that similar trends exist with respect to the fitting curves for monovalent ions from the previous work of Joung and Cheatham:[22] HFE increases with a decrease in $R_{min}/2$ and smaller $R_{min}/2$ values with a large ε can yield similar HFEs as a larger $R_{min}/2$ parameter coupled with a smaller ε value. This can be explained by the form of the LJ potential

Table 5. Comparison of Results of Different Scaling Methods in the VDW-Disappearing and Appearing Steps of the HFE Calculation for the Be^{2+} and Ba^{2+} Ions[a]

		VDW-appearing				VDW-disappearing			
		L	K4	K6	SC	L	K4	K6	SC
Be^{2+}	3 windows				0.44				−0.45
	5 windows	0.25	0.19	0.17		−0.26	−0.38	−0.38	
	7 windows	0.28	0.24	0.23		−0.29	−0.38	−0.39	
	9 windows	0.30	0.27	0.25		−0.29	−0.39	−0.37	
Ba^{2+}	3 windows				1.56				−1.41
	5 windows	−0.40	−1.34	−1.74		0.54	−2.08	−1.76	
	7 windows	0.12	−0.74	−1.10		0.05	−1.83	−1.90	
	9 windows	0.31	−0.45	−0.59		−0.18	−1.74	−1.95	

[a]In kcal/mol.

dx.doi.org/10.1021/ct400146w | J. Chem. Theory Comput. 2013, 9, 2733−2748

Table 6. Final Optimized HFE LJ Parameter Sets for Different Water Models

	TIP3P		SPC/E		$TIP4P_{EW}$	
	$R_{min}/2$ (Å)	ε(kcal/mol)	$R_{min}/2$ (Å)	ε(kcal/mol)	$R_{min}/2$ (Å)	ε(kcal/mol)
Be^{2+}	0.907	0.00000080	0.915	0.00000105	0.815	0.0000000221
Cu^{2+}	1.144	0.00040203	1.149	0.00044254	1.078	0.00010063
Ni^{2+}	1.162	0.00056491	1.166	0.00060803	1.101	0.00016733
Pt^{2+}	1.173	0.00069036	1.176	0.00072849	1.114	0.00022027
Zn^{2+}	1.175	0.00071558	1.178	0.00075490	1.115	0.00022490
Co^{2+}	1.211	0.00132548	1.217	0.00146124	1.141	0.00037931
Pd^{2+}	1.215	0.00141473	1.217	0.00146124	1.145	0.00040986
Ag^{2+}	1.263	0.00294683	1.265	0.00303271	1.171	0.00066591
Cr^{2+}	1.273	0.00339720	1.276	0.00354287	1.181	0.00079606
Fe^{2+}	1.277	0.00359255	1.284	0.00395662	1.194	0.00099751
Mg^{2+}	1.284	0.00395662	1.288	0.00417787	1.208	0.00126172
V^{2+}	1.290	0.00429223	1.293	0.00446856	1.210	0.00130393
Mn^{2+}/Hg^{2+}	1.339	0.00799176	1.338	0.00789684	1.276	0.00354287
Cd^{2+}	1.339	0.00799176	1.344	0.00848000	1.279	0.00369364
Yb^{2+}	1.526	0.04772212	1.518	0.04490976	1.464	0.02883819
Ca^{2+}	1.528	0.04844326	1.520	0.04560206	1.467	0.02960343
Sn^{2+}	1.543	0.05408454	1.532	0.04990735	1.479	0.03280986
Pb^{2+}	1.620	0.08965674	1.609	0.08389240	1.551	0.05726270
Eu^{2+}	1.666	0.11617738	1.656	0.11008622	1.596	0.07737276
Sr^{2+}	1.672	0.11991675	1.659	0.11189491	1.606	0.08235966
Sm^{2+}	1.680	0.12499993	1.667	0.11679623	1.606	0.08235966
Ba^{2+}/Ra^{2+}	1.842	0.24821230	1.825	0.23380842	1.768	0.18767274

Table 7. Final Optimized IOD LJ Parameter Set[a]

	$R_{min}/2$ (Å)	ε(kcal/mol)
Be^{2+}	1.168	0.00063064
Cu^{2+}	1.409	0.01721000
Ni^{2+}	1.373	0.01179373
Zn^{2+}	1.395	0.01491700
Co^{2+}	1.404	0.01636246
Cr^{2+}	1.388	0.01386171
Fe^{2+}	1.409	0.01721000
Mg^{2+}	1.395	0.01491700
V^{2+}	1.476	0.03198620
Mn^{2+}	1.467	0.02960343
Hg^{2+}	1.575	0.06751391
Cd^{2+}	1.506	0.04090549
Ca^{2+}	1.608	0.08337961
Sn^{2+}	1.738	0.16500296
Sr^{2+}	1.753	0.17618319
Ba^{2+}	1.913	0.31060194

[a]The parameters are the same for the different water models.

function (see eq 10): since $A = \varepsilon^* r_{min}^{12}$ and $B = 2\varepsilon^* r_{min}^{6}$, smaller $R_{min}/2$ parameters with bigger ε values and smaller ε parameters with larger $R_{min}/2$ values yield similar A and B values.[79] Furthermore, ε is directly proportional to A and B while R_{min} /2 is raised to the twelfth and sixth power in the expression for A and B, respectively. This is the reason why the HFE is quasi-linearly dependent on $R_{min}/2$ while the dependency in ε is logarithmic.

$$U_{ij} = \frac{A}{r_{ij}^{12}} - \frac{B}{r_{ij}^{6}} = \varepsilon\left[\left(\frac{r_{min}}{r_{ij}}\right)^{12} - 2\left(\frac{r_{min}}{r_{ij}}\right)^{6}\right] \quad (10)$$

Figure 2 shows that, generally, all of the fitting curves have a similar shape but different Y-intercepts for the TIP3P water model. The HFE fitting curves for the other three water models (Figure SI.1) exhibited similar behavior. The data in Table SI.3 show that the HFE differences for the same LJ parameters within different water models could not be neglected. To specify these differences in a more distinct way, we treated Zn^{2+} ion as an example and give its HFE fitting curves with the four different water models in Figure 3. It can be seen that the two three-site models (TIP3P and SPC/E) show very similar results and are distinctly different from the two 4-site models (TIP4P and $TIP4P_{EW}$). The two four-site water models also showed a remarkable difference from each other. Therefore, we concluded it is necessary for us to design different parameters for the same metal ions for use with different water models.

Meanwhile, Table SI.4 shows that the four water models generated very similar IOD values and CNs for the same LJ parameters. To elucidate the difference in IOD values for the four studied water models, we carried out a standard deviation analysis of the IOD values between each pair of the four water models and display the data in Table 3. Our results indicate the TIP3P and SPC/E water models have nearly the same IOD values with a 0.00 Å systematic difference and 0.01 Å standard deviation with each other when using the same LJ parameters for the metal ions while a similar situation exists between the TIP4P and $TIP4P_{EW}$ water models. Generally, there is a 0.02 Å systematic difference between the three-site and four-site water models for the IOD values when the same LJ parameters are utilized for the metal ions. Meanwhile, IOD fitting curves were obtained from Table SI.4 by following the same procedures as for the HFE fitting curves. Again, we treated the Zn^{2+} ion as an example and depict the IOD fitting curves in Figure 4 (other examples such as Cd^{2+} and Ba^{2+} ions are shown in Figure SI.2 in SI). It can be seen from the figure that the two three-site water models share one curve and the two four-site water models share the other curve, although in the latter instance there is a slight difference, in agreement with the standard deviation analysis (Table 3).

Table 8. Final Optimized CM Parameters Sets for the Different Water Models

	TIP3P		SPC/E		TIP4P$_{EW}$	
	$R_{min}/2$ (Å)	ε(kcal/mol)	$R_{min}/2$ (Å)	ε(kcal/mol)	$R_{min}/2$ (Å)	ε(kcal/mol)
Be^{2+}	0.956	0.00000395	0.961	0.00000460	0.918	0.00000116
Cu^{2+}	1.218	0.00148497	1.223	0.00160860	1.195	0.00101467
Ni^{2+}	1.255	0.00262320	1.253	0.00254709	1.221	0.00155814
Pt^{2+}	1.266	0.00307642	1.272	0.00334975	1.251	0.00247282
Zn^{2+}	1.271	0.00330286	1.276	0.00354287	1.252	0.00250973
Co^{2+}	1.299	0.00483892	1.305	0.00523385	1.288	0.00417787
Pd^{2+}	1.303	0.00509941	1.305	0.00523385	1.288	0.00417787
Ag^{2+}	1.336	0.00770969	1.337	0.00780282	1.323	0.00657749
Cr^{2+}	1.346	0.00868178	1.348	0.00888732	1.333	0.00743559
Fe^{2+}	1.353	0.00941798	1.354	0.00952704	1.343	0.00838052
Mg^{2+}	1.360	0.01020237	1.360	0.01020237	1.353	0.00941798
V^{2+}	1.364	0.01067299	1.365	0.01079325	1.353	0.00941798
Mn^{2+}/Hg^{2+}	1.407	0.01686710	1.406	0.01669760	1.401	0.01586934
Cd^{2+}	1.412	0.01773416	1.412	0.01773416	1.406	0.01669760
Yb^{2+}	1.642	0.10185975	1.634	0.09731901	1.654	0.10888937
Ca^{2+}	1.649	0.10592870	1.635	0.09788018	1.657	0.11068733
Sn^{2+}	1.666	0.11617738	1.651	0.10710756	1.670	0.11866330
Pb^{2+}	1.745	0.17018074	1.731	0.15989650	1.758	0.17997960
Eu^{2+}	1.802	0.21475916	1.786	0.20184160	1.823	0.23213110
Sr^{2+}	1.810	0.22132374	1.794	0.20826406	1.827	0.23548950
Sm^{2+}	1.819	0.22878796	1.800	0.21312875	1.838	0.24480038
Ba^{2+}/ Ra^{2+}	2.019	0.40664608	1.980	0.37126402	2.050	0.43454345

As discussed in the Introduction, the nonbonded model can simulate the CN switching processes. There are several noninteger CNs in Table SI.4, which suggests there is CN switching occurring during the simulations. As an example, we show CN switching in the MD simulation of a M(II) metal ion with LJ parameters of $R_{min}/2$ = 2.2 Å and ε = 0.1 kcal/mol in a TIP3P water box in Figure 5. We observe the CN switching between eight, nine, ten and eleven water molecules during the simulation. Other examples of CN switching are shown in Figure SI.3, which includes CN switching between two, three, and four water molecules when $R_{min}/2$ = 1.2 Å and ε = 10^{-6} kcal/mol, CN switching between four, five, and six water molecules when $R_{min}/2$ = 0.9 Å and ε = 0.01 kcal/mol, and CN switching between seven and eight water molecules when $R_{min}/2$ = 2.1 Å and ε = 10^{-3} kcal/mol of the M(II) metal ion in TIP3P water box.

A detailed examination of the results contained in Tables SI.3 and SI.4 reveals that, for each water model, for the points corresponding to the same HFE, they have almost the same IOD and CN. These results suggest there is likely a relationship between the HFE, IOD, and CN values for the metal ion−water systems, hinting at the strong correlation between the various solvation properties, which is consistent with earlier work.[79] Figure 6 shows the HFE and IOD fitting curves for six representative metal ions with different sizes in TIP3P water while Figure SI.4 depicts the HFE and IOD fitting curves for these metal ions in SPC/E, TIP4P and TIP4P$_{EW}$ water models. From Figure 6 we find that the IOD and HFE fitting curves for each metal ion are almost parallel with each other and do not have any intersection points in the investigated range, implying it is hard to find a parameter to reproduce the experimental HFE and IOD values at the same time for these metal ions. At the same time, the figure also shows that the difference between the HFE and IOD fitting curves of metal ion begins to decrease along with increasing metal ion size, which may be due to the simplicity of the nonbonded model. The electrostatic plus LJ potential approximation underestimates the interaction energy of the metal ion and ligating residues at short-range, especially when there is strong charge transfer, polarization, or even covalent interaction between them. In this situation, if one wants to reproduce the experimental HFEs, one should have shorter IOD values than the experimental values. Meanwhile, the nonbonded model is more appropriate for the monovalent metal ions since polarization and charge transfer effects likely decrease (and these ions tend to be mostly ionic in nature) allowing the parameters to be designed to fit both experimental HFE and IOD values simultaneously.[22]

Therefore, there appears to be no single "perfect" LJ parameter set for the M(II) ions since none are able to reproduce the experimental HFE and IOD values simultaneously in a simulation. Hence, we concluded that it was necessary to design several sets of parameters for these M(II) metal ions to meet different demands. Since our intention is to design LJ parameters for the M(II) metal ions specifically for PME based MD simulations, we only designed parameters for the TIP3P, SPC/E, and TIP4P$_{EW}$ water models. The TIP4P water model was modified to produce the TIP4P$_{EW}$ model, which is designed specifically for PME based simulations.[62] First, by treating the experimental HFEs as the target property, we designed the HFE set of parameters for each of the three water models. Next, we designed the IOD set of parameters to reproduce the experimental IOD values (due to the limited experimental data set for IOD values, only 16 of 24 ions have IOD parameter sets). In the case of the IOD parameter sets, they ended up being the same for the three water models. In the end, we designed the CM (short for compromise) set of parameters for the three water models respectively, which is a compromise between the HFE and IOD sets using the experimental relative HFEs and CNs as targets. During our parametrization efforts, we found that it was impossible to simulate all the CNs while simultaneously reproducing the relative HFEs for the CM set of parameters so we

Table 9a. Simulated HFE, IOD, and CN Values for the Parameters Given in Table 6 (HFE Set)[a]

	TIP3P				SPC/E				TIP4P$_{EW}$			
	HFE (kcal/mol)	relative HFE (M^{2+}-Cd^{2+}) (kcal/mol)	IOD (Å)	CN	HFE (kcal/mol)	relative HFE (M^{2+}-Cd^{2+}) (kcal/mol)	IOD (Å)	CN	HFE (kcal/mol)	relative HFE (M^{2+}-Cd^{2+}) (kcal/mol)	IOD (Å)	CN
Be^{2+}	−572.3	−152.5	1.14	2.0	−571.4	−152.4	1.15	2.0	−572.8	−153.2	0.87	1.0
Cu^{2+}	−481.2	−61.4	1.63	4.0	−481.2	−62.2	1.64	4.0	−481.1	−61.5	1.57	4.0
Ni^{2+}	−473.0	−53.2	1.65	4.0	−473.2	−54.2	1.66	4.0	−472.4	−52.8	1.60	4.0
Pt^{2+}	−467.8	−48.0	1.67	4.1	−468.4	−49.4	1.67	4.1	−468.0	−48.4	1.61	4.0
Zn^{2+}	−467.4	−47.6	1.67	4.1	−467.3	−48.3	1.68	4.3	−467.4	−47.8	1.61	4.0
Co^{2+}	−457.0	−37.2	1.87	6.0	−456.9	−37.9	1.89	6.0	−458.6	−39.0	1.64	4.0
Pd^{2+}	−457.0	−37.2	1.88	6.0	−456.8	−37.8	1.89	6.0	−456.1	−36.5	1.65	4.0
Ag^{2+}	−445.0	−25.2	1.93	6.0	−446.0	−27.0	1.94	6.0	−445.2	−25.6	1.69	4.1
Cr^{2+}	−441.6	−21.8	1.94	6.0	−441.9	−22.9	1.95	6.0	−442.3	−22.7	1.84	5.6
Fe^{2+}	−439.5	−19.7	1.94	6.0	−439.4	−20.4	1.96	6.0	−440.4	−20.8	1.88	6.0
Mg^{2+}	−437.7	−17.9	1.95	6.0	−437.6	−18.6	1.96	6.0	−436.5	−16.9	1.89	6.0
V^{2+}	−435.9	−16.1	1.95	6.0	−435.8	−16.8	1.96	6.0	−435.6	−16.0	1.90	6.0
Mn^{2+}	−419.9	−0.1	2.01	6.0	−420.6	−1.6	2.01	6.0	−419.9	−0.3	1.96	6.0
Hg^{2+}	−419.9	−0.1	2.01	6.0	−420.6	−1.6	2.01	6.0	−419.9	−0.3	1.96	6.0
Cd^{2+}	−419.8	0.0	2.01	6.0	−419.0	0.0	2.02	6.0	−419.6	0.0	1.96	6.0
Yb^{2+}	−360.2	59.6	2.33	7.4	−360.2	58.8	2.30	7.0	−361.3	58.3	2.19	6.1
Ca^{2+}	−360.2	59.6	2.33	7.4	−360.6	58.4	2.31	7.0	−359.8	59.8	2.20	6.2
Sn^{2+}	−356.5	63.3	2.36	7.7	−356.4	62.6	2.33	7.2	−356.2	63.4	2.23	6.5
Pb^{2+}	−340.9	78.9	2.46	8.0	−340.4	78.6	2.45	7.9	−339.7	79.9	2.39	7.7
Eu^{2+}	−331.2	88.6	2.51	8.0	−330.9	88.1	2.51	8.0	−331.0	88.6	2.45	7.9
Sr^{2+}	−329.7	90.1	2.52	8.1	−330.6	88.4	2.51	8.0	−329.5	90.1	2.46	8.0
Sm^{2+}	−328.4	91.4	2.53	8.1	−328.6	90.4	2.52	8.0	−328.8	90.8	2.46	8.0
Ba^{2+}	−299.4	120.4	2.74	9.0	−299.2	119.8	2.72	8.8	−299.1	120.5	2.67	8.8
Ra^{2+}	−299.4	120.4	2.74	9.0	−299.2	119.8	2.72	8.8	−299.1	120.5	2.67	8.8
avg. error	0.1	0.4	−0.27	−0.4	0.0	−0.5	−0.26	−0.5	0.1	0.2	−0.36	−0.8
SD	0.5	0.5	0.14	1.0	0.5	0.5	0.14	1.0	0.5	0.5	0.17	1.1
unsigned avg. error	0.4	0.5	0.27	0.6	0.4	0.6	0.26	0.6	0.5	0.4	0.36	0.9

[a]All the average errors and standard deviations were obtained by treating the corresponding experimental values as the standard (see Table 1). For the average error and standard deviation (SD) of simulated IOD values the average experimental IOD values of each metal ion were treated as the reference.

compromised on the reproduction of the CNs for the Be^{2+} and Sn^{2+} ions and tried to best reproduce their relative HFE values. This leads to the CM parameter set having an average error of ~25 kcal/mol in the absolute HFE (while reproducing the relative HFE) for the TIP3P and SPC/E water models, while for the TIP4P$_{EW}$ water model this value increased to ~40 kcal/mol.

How to Find Reasonable LJ Parameters. Although numerous points exist on the fitting curves capable of reproducing almost the same HFE, IOD, and CN values, it is still problematic to pick a single point among them to determine the final LJ parameters. Initially, we wanted to do simulations on the solid-state salts of these M(II) metal ions together with anions for the different combinations of LJ parameters, as employed in the protocol of Joung and Cheatham.[22] However, it is difficult to find valid and consistent experimental data for the salts containing the M(II) metal ions we are dealing with. Our second approach was to pick the point capable of also reproducing the QM calculated interaction energy between one metal ion with one or several surrounding water molecules. Unfortunately, we could not obtain reasonable results for all the metal ions, which likely reflects the simplicity of the nonbonded model. Although for some metal ions (such as Ca^{2+}) we could get reasonable results, we could not obtain valid results for most of the ions, especially for the metal ions capable of strong covalent interactions with the surrounding waters. Furthermore, it also proved difficult to find a standard QM method protocol largely due to the various electronic states possible for some of the metal ions.

Finally, we selected an alternate way to design the 6−12 LJ parameters. The LJ potential, which was first proposed by Sir John Edward Lennard-Jones to represent the interaction between noble gas atoms in 1924 was remarkably accurate for the noble gases and a very good approximation for neutral atoms and molecules.[80] In the function the r^{-12} term represents the interaction caused by Pauli Repulsion due to the overlap of the molecular orbitals at close distance. The r^{-6} term describes the attraction between the molecules in the long-range due to the dispersion force. Generally, the more dispersive electronic cloud one particle has, the bigger $R_{min}/2$ and ε value it should have, which is consistent with the experimental data.[81] Using the experimental data[81] and the Lorentz−Berthelot combing rules, we obtained the ε and $R_{min}/2$ values for the He, Ne, Ar, Kr, and Xe atoms (Table 4). For all of the metal ions treated here, they should have smaller $R_{min}/2$ and ε values than those of Xe since the biggest metal ion herein, Ba^{2+} has a smaller $R_{min}/2$ than Xe because of the same electronic structure but a larger nuclear charge. Furthermore, if one metal ion's $R_{min}/2$ value is between that of Kr and Xe atoms, its ε values should be in the range of the ε values of the Kr and Xe atoms as well. Moreover, if we could get a curve to represent the relationship between $R_{min}/2$ and ε, together with the HFE and IOD fitting

Table 9b. Simulated HFE, IOD, and CN Values for the Parameters Given in Table 7 (IOD Set)[a]

	TIP3P				SPC/E				TIP4P				TIP4P$_{EW}$			
	HFE (kcal/mol)	relative HFE (M^{2+}-Cd^{2+}) (kcal/mol)	IOD (Å)	CN	HFE (kcal/mol)	relative HFE (M^{2+}-Cd^{2+}) (kcal/mol)	IOD (Å)	CN	HFE (kcal/mol)	relative HFE (M^{2+}-Cd^{2+}) (kcal/mol)	IOD (Å)	CN	HFE (kcal/mol)	relative HFE (M^{2+}-Cd^{2+}) (kcal/mol)	IOD (Å)	CN
Be^{2+}	−469.8	−103.9	1.66	4.0	−472.0	−108.1	1.66	4.0	−435.0	−91.9	1.68	4.4	−446.8	−97.3	1.68	4.0
Cu^{2+}	−395.2	−29.3	2.10	6.0	−395.4	−31.5	2.10	6.0	−368.7	−25.6	2.11	6.0	−378.6	−29.1	2.12	6.0
Ni^{2+}	−407.6	−41.7	2.05	6.0	−408.2	−44.3	2.05	6.0	−380.9	−37.8	2.07	6.0	−390.4	−40.9	2.07	6.0
Zn^{2+}	−400.0	−34.1	2.08	6.0	−400.0	−36.1	2.08	6.0	−373.5	−30.4	2.10	6.0	−382.0	−32.5	2.10	6.0
Co^{2+}	−397.0	−31.1	2.09	6.0	−397.1	−33.2	2.09	6.0	−370.7	−27.6	2.11	6.0	−379.6	−30.1	2.11	6.0
Cr^{2+}	−402.8	−36.9	2.07	6.0	−403.2	−39.3	2.07	6.0	−376.0	−32.9	2.09	6.0	−385.0	−35.5	2.09	6.0
Fe^{2+}	−394.8	−28.9	2.10	6.0	−395.3	−31.4	2.10	6.0	−369.3	−26.2	2.11	6.0	−378.4	−28.9	2.12	6.0
Mg^{2+}	−400.3	−34.4	2.08	6.0	−400.5	−36.6	2.08	6.0	−373.9	−30.8	2.09	6.0	−382.9	−33.4	2.10	6.0
V^{2+}	−372.8	−6.9	2.21	6.6	−372.2	−8.3	2.19	6.1	−349.5	−6.4	2.26	7.0	−356.2	−6.7	2.22	6.3
Mn^{2+}	−375.6	−9.7	2.18	6.3	−375.4	−11.5	2.18	6.0	−351.6	−8.5	2.22	6.6	−359.9	−10.4	2.20	6.1
Hg^{2+}	−350.1	15.8	2.41	7.9	−346.4	17.5	2.40	7.6	−329.4	13.7	2.42	8.0	−335.1	14.4	2.42	7.9
Cd^{2+}	−365.9	0.0	2.29	7.1	−363.9	0.0	2.28	6.8	−343.1	0.0	2.31	7.4	−349.5	0.0	2.31	7.1
Ca^{2+}	−342.3	23.6	2.45	8.0	−340.6	23.3	2.45	7.9	−323.3	19.8	2.46	8.0	−329.2	20.3	2.47	8.0
Sn^{2+}	−317.6	48.3	2.61	8.6	−314.8	49.1	2.61	8.2	−299.8	43.3	2.63	8.8	−305.2	44.3	2.63	8.6
Sr^{2+}	−314.2	51.7	2.63	8.6	−311.8	52.1	2.62	8.3	−297.7	45.4	2.65	8.8	−301.7	47.8	2.65	8.7
Ba^{2+}	−288.2	77.7	2.82	9.2	−285.1	78.8	2.82	9.0	−273.3	69.8	2.84	9.4	−276.9	72.6	2.84	9.2
avg. error	51.1	−2.5	−0.01	0.4	51.9	−3.7	−0.01	0.3	74.8	−1.6	0.01	0.5	67.2	−2.8	0.01	0.4
SD	25.2	25.2	0.00	0.8	24.3	24.3	0.00	0.7	29.3	29.3	0.01	0.9	27.5	27.5	0.00	0.8
unsigned avg. error	51.1	20.0	0.01	0.4	51.9	19.7	0.01	0.3	74.8	22.3	0.01	0.5	67.2	21.5	0.01	0.4

[a]All the average errors and standard deviations were obtained by treating the corresponding experimental values as the standard (See Table 1). For the average error and standard deviation (SD) of simulated IOD values the average experimental IOD values of each metal ions were treated as the reference.

dx.doi.org/10.1021/ct400146w | J. Chem. Theory Comput. 2013, 9, 2733−2748

Table 9c. Simulated HFE, IOD, and CN Values for the Parameters Given in Table 8 (CM Set)[a]

	TIP3P				SPC/E				TIP4P$_{EW}$			
	HFE (kcal/mol)	relative HFE (M^{2+}-Cd^{2+}) (kcal/mol)	IOD (Å)	CN	HFE (kcal/mol)	relative HFE (M^{2+}-Cd^{2+}) (kcal/mol)	IOD (Å)	CN	HFE (kcal/mol)	relative HFE (M^{2+}-Cd^{2+}) (kcal/mol)	IOD (Å)	CN
Be^{2+}	−547.3	−153.7	1.21	2.0	−547.5	−153.0	1.22	2.0	−532.2	−153.6	1.17	2.0
Cu^{2+}	−455.0	−61.4	1.88	6.0	−454.6	−60.1	1.90	6.0	−439.9	−61.3	1.88	6.0
Ni^{2+}	−447.9	−54.3	1.92	6.0	−448.4	−53.9	1.92	6.0	−432.4	−53.8	1.91	6.0
Pt^{2+}	−443.7	−50.1	1.93	6.0	−443.8	−49.3	1.94	6.0	−427.8	−49.2	1.94	6.0
Zn^{2+}	−442.0	−48.4	1.93	6.0	−441.6	−47.1	1.95	6.0	−427.8	−49.2	1.94	6.0
Co^{2+}	−433.0	−39.4	1.96	6.0	−431.9	−37.4	1.98	6.0	−416.8	−38.2	1.97	6.0
Pd^{2+}	−431.5	−37.9	1.97	6.0	−432.2	−37.7	1.98	6.0	−416.8	−38.2	1.97	6.0
Ag^{2+}	−420.8	−27.2	2.00	6.0	−420.4	−25.9	2.01	6.0	−405.1	−26.5	2.01	6.0
Cr^{2+}	−417.3	−23.7	2.02	6.0	−417.0	−22.5	2.03	6.0	−403.1	−24.5	2.02	6.0
Fe^{2+}	−414.6	−21.0	2.02	6.0	−415.3	−20.8	2.03	6.0	−400.0	−21.4	2.03	6.0
Mg^{2+}	−412.1	−18.5	2.03	6.0	−412.8	−18.3	2.04	6.0	−396.4	−17.8	2.05	6.0
V^{2+}	−410.7	−17.1	2.04	6.0	−411.4	−16.9	2.05	6.0	−395.6	−17.0	2.05	6.0
Mn^{2+}	−396.1	−2.5	2.09	6.0	−396.5	−2.0	2.10	6.0	−380.7	−2.1	2.11	6.0
Hg^{2+}	−396.1	−2.5	2.09	6.0	−396.5	−2.0	2.10	6.0	−380.7	−2.1	2.11	6.0
Cd^{2+}	−393.6	0.0	2.10	6.0	−394.5	0.0	2.10	6.0	−378.6	0.0	2.11	6.0
Yb^{2+}	−335.7	57.9	2.48	8.0	−335.3	59.2	2.48	8.0	−320.1	58.5	2.52	8.0
Ca^{2+}	−334.6	59.0	2.49	8.0	−334.5	60.0	2.48	8.0	−319.0	59.6	2.53	8.0
Sn^{2+}	−331.2	62.4	2.51	8.1	−331.5	63.0	2.50	8.0	−316.4	62.2	2.54	8.1
Pb^{2+}	−316.2	77.4	2.62	8.7	−315.7	78.8	2.60	8.2	−301.3	77.3	2.66	8.7
Eu^{2+}	−305.8	87.8	2.69	8.9	−305.2	89.3	2.67	8.5	−290.6	88.0	2.74	8.9
Sr^{2+}	−304.9	88.7	2.70	8.9	−304.5	90.0	2.68	8.6	−289.6	89.0	2.74	8.9
Sm^{2+}	−303.0	90.6	2.71	8.9	−302.7	91.8	2.69	8.6	−288.1	90.5	2.75	9.0
Ba^{2+}	−273.1	120.5	2.94	9.7	−274.7	119.8	2.90	9.2	−258.4	120.2	3.00	9.9
Ra^{2+}	−273.1	120.5	2.94	9.7	−274.7	119.8	2.90	9.2	−258.4	120.2	3.00	9.9
avg. error	25.1	−0.8	−0.13	0.0	25.0	0.0	−0.12	0.0	40.3	−0.6	−0.11	0.1
SD	0.4	0.4	0.14	0.8	0.6	0.6	0.13	0.7	0.5	0.5	0.16	0.8
unsigned svg. error	25.1	0.8	0.15	0.3	25.0	0.5	0.14	0.3	40.3	0.6	0.16	0.3

[a]All the average errors and standard deviations were obtained by treating the corresponding experimental values as the standard (see Table 1). For the average error and standard deviation (SD) of simulated IOD values the average experimental IOD values of each metal ions were treated as the reference.

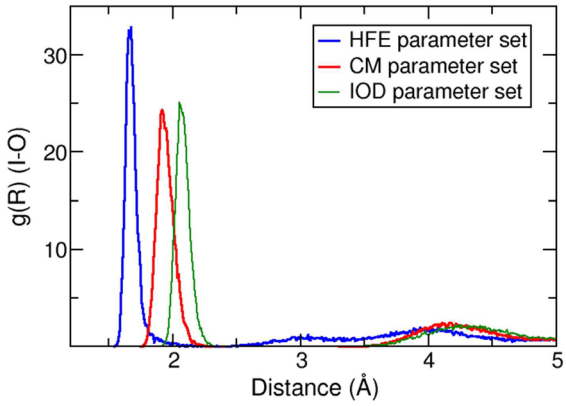

Figure 8. Radial distribution functions of three sets of parameters for Zn^{2+} ion in TIP3P.

curves we obtained in the former part, we could determine the LJ parameters for the M(II) metal ions.

To be consistent with the HFE and IOD fitting curves, we produced the curve fittings between $-\log(\varepsilon)$ and $R_{min}/2$ shown in Table 4. By treating $f(x) = -\log(\varepsilon)$ and $x = R_{min}/2$, we attempted several fits with different functions. Finally, we found that the Slater function $f(x) = C_1 \times e^{-C_2 x}$ with $C_1 = 57.36$ and $C_2 = 2.471$ had a better R^2 value (0.98265) than the quadratic fitting ($R^2 = 0.94509$). We named the curve the Noble Gas Curve (NGC) and determined the final LJ parameters from the points on this curve.

Table 10. Comparison of the $R_{min}/2$ Values Determined Herein with Earlier Values

	$R_{min}/2$ determined for TIP3P water model by Joung and Cheatham[22] (Å)	$R_{min}/2$ of HFE parameter set determined for TIP3P water model in this work (Å)	VDW radius determined by Stokes[82] (Å)
Li^+	1.205		
Be^{2+}		0.907	
Na^+	1.369		1.352
Mg^{2+}		1.284	1.180
K^+	1.705		1.671
Ca^{2+}		1.528	1.480
Rb^+	1.813		1.801
Sr^{2+}		1.672	1.625
Cs^+	1.976		1.997
Ba^{2+}		1.842	1.802

Final Determination of the LJ Parameters. The HFE, CM, and IOD fitting curves for the Zn^{2+} ion and the NGC are shown in Figure 7. It can be seen that the CM fitting curve for the Zn^{2+} ion is almost in the middle of the HFE and IOD fitting curves. The original LJ parameters can be obtained as the intersection points between the HFE, CM, and IOD fitting

Table 11a. Percent Errors of Three Parameter Sets Toward the Experimental HFEs[a]

	TIP3P	SPCE	TIP4P$_{EW}$	TIP4P
Be^{2+}	0.0%(−4.4%)[−17.9%]	−0.2%(−4.4%)[−17.5%]	0.1%(−7.0%)[−21.9%]	—(—)[−24.0%]
Cu^{2+}	0.2%(−5.3%)[−17.7%]	0.2%(−5.4%)[−17.7%]	0.1%(−8.4%)[−21.2%]	—(—)[−23.3%]
Ni^{2+}	0.0%(−5.3%)[−13.9%]	0.0%(−5.2%)[−13.7%]	−0.2%(−8.6%)[−17.5%]	—(—)[−19.5%]
Pt^{2+}	−0.1%(−5.3%)[—]	0.0%(−5.3%)[—]	−0.1%(−8.7%)[—]	
Zn^{2+}	0.0%(−5.4%)[−14.4%]	0.0%(−5.5%)[−14.4%]	0.0%(−8.5%)[−18.3%]	—(—)[−20.1%]
Co^{2+}	−0.2%(−5.4%)[−13.3%]	−0.2%(−5.6%)[−13.2%]	0.2%(−8.9%)[−17.1%]	—(—)[−19.0%]
Pd^{2+}	0.1%(−5.5%)[—]	0.1%(−5.3%)[—]	−0.1%(−8.7%)[—]	
Ag^{2+}	−0.2%(−5.6%)[—]	0.1%(−5.7%)[—]	−0.1%(−9.1%)[—]	
Cr^{2+}	−0.1%(−5.6%)[−8.9%]	−0.1%(−5.7%)[−8.8%]	0.0%(−8.8%)[−12.9%]	—(—)[−15.0%]
Fe^{2+}	−0.1%(−5.7%)[−10.2%]	−0.1%(−5.6%)[−10.1%]	0.1%(−9.0%)[−14.0%]	—(—)[−16.0%]
Mg^{2+}	0.1%(−5.8%)[−8.5%]	0.0%(−5.6%)[−8.4%]	−0.2%(−9.4%)[−12.5%]	—(—)[−14.5%]
V^{2+}	−0.1%(−5.8%)[−14.5%]	−0.1%(−5.7%)[−14.7%]	−0.1%(−9.3%)[−18.3%]	—(—)[−19.9%]
Mn^{2+}	−0.2%(−5.8%)[−10.7%]	0.0%(−5.8%)[−10.8%]	−0.2%(−9.5%)[−14.5%]	—(—)[−16.4%]
Hg^{2+}	−0.2%(−5.8%)[−16.8%]	0.0%(−5.8%)[−17.7%]	−0.2%(−9.5%)[−20.3%]	—(—)[−21.7%]
Cd^{2+}	0.1%(−6.2%)[−12.8%]	−0.1%(−6.0%)[−13.3%]	0.0%(−9.7%)[−16.7%]	—(—)[−18.2%]
Yb^{2+}	−0.2%(−7.0%)[—]	−0.2%(−7.1%)[—]	0.1%(−11.3%)[—]	
Ca^{2+}	0.1%(−7.0%)[−4.8%]	0.3%(−7.0%)[−5.3%]	0.0%(−11.3%)[−8.5%]	—(—)[−10.1%]
Sn^{2+}	0.1%(−7.0%)[−10.8%]	0.1%(−6.9%)[−11.6%]	0.0%(−11.1%)[−14.3%]	—(—)[−15.8%]
Pb^{2+}	0.1%(−7.2%)[—]	−0.1%(−7.3%)[—]	−0.3%(−11.5%)[—]	
Eu^{2+}	0.1%(−7.6%)[—]	0.0%(−7.8%)[—]	0.0%(−12.2%)[—]	
Sr^{2+}	0.0%(−7.6%)[−4.7%]	0.2%(−7.7%)[−5.5%]	−0.1%(−12.2%)[−8.5%]	—(—)[−9.7%]
Sm^{2+}	−0.1%(−7.8%)[—]	0.0%(−7.9%)[—]	0.1%(−12.3%)[—]	
Ba^{2+}	0.2%(−8.6%)[−3.5%]	0.1%(−8.1%)[−4.6%]	0.1%(−13.5%)[−7.3%]	—(—)[−8.5%]
Ra^{2+}	0.2%(−8.6%)[—]	0.1%(−8.1%)[—]	0.1%(−13.5%)[—]	
avg. value	0.0%(−6.3%)[−11.5%]	0.0%(−6.3%)[−11.7%]	0.0%(−10.1%)[−15.2%]	—(—)[−17.0%]
SD	0.1%(1.1%)[4.5%]	0.1%(1.1%)[4.3%]	0.1%(1.8%)[4.5%]	—(—)[4.7%]

[a]The first values in the cells are for the HFE parameter set, the values in parentheses are for the CM parameter set while the ones in square brackets are for the IOD parameter set. Some values are shown as blank because we did not design IOD parameter set for some M(II) metal ions due to lack of the corresponding experimental values and we only design the IOD parameter set for TIP4P water model.

Table 11b. Percent Errors of Three Parameter Sets Towards the Experimental IOD Values[a]

	TIP3P	SPCE	TIP4P$_{EW}$	TIP4P
Be^{2+}	−31.7%(−27.5%)[−0.6%]	−31.1%(−26.9%)[−0.6%]	−47.9%(−29.9%)[0.6%]	—(—)[0.6%]
Cu^{2+}	−22.7%(−10.9%)[−0.5%]	−22.3%(−10.0%)[−0.5%]	−25.6%(−10.9%)[0.5%]	—(—)[0.0%]
Ni^{2+}	−19.9%(−6.8%)[−0.5%]	−19.4%(−6.8%)[−0.5%]	−22.3%(−7.3%)[0.5%]	—(—)[0.5%]
Zn^{2+}	−20.1%(−7.7%)[−0.5%]	−19.6%(−6.7%)[−0.5%]	−23.0%(−7.2%)[0.5%]	—(—)[0.5%]
Co^{2+}	−11.0%(−6.7%)[−0.5%]	−10.0%(−5.7%)[−0.5%]	−21.9%(−6.2%)[0.5%]	—(—)[0.5%]
Cr^{2+}	−6.7%(−2.9%)[−0.5%]	−6.3%(−2.4%)[−0.5%]	−11.5%(−2.9%)[0.5%]	—(—)[0.5%]
Fe^{2+}	−8.1%(−4.3%)[−0.5%]	−7.1%(−3.8%)[−0.5%]	−10.9%(−3.8%)[0.5%]	—(—)[0.0%]
Mg^{2+}	−6.7%(−2.9%)[−0.5%]	−6.2%(−2.4%)[−0.5%]	−9.6%(−1.9%)[0.5%]	—(—)[0.0%]
V^{2+}	−11.8%(−7.7%)[0.0%]	−11.3%(−7.2%)[−0.9%]	−14.0%(−7.2%)[0.5%]	—(—)[2.3%]
Mn^{2+}	−8.2%(−4.6%)[−0.5%]	−8.2%(−4.1%)[−0.5%]	−10.5%(−3.7%)[0.5%]	—(—)[1.4%]
Hg^{2+}	−16.6%(−13.3%)[0.0%]	−16.6%(−12.9%)[−0.4%]	−18.7%(−12.4%)[0.4%]	—(—)[0.4%]
Cd^{2+}	−12.6%(−8.7%)[−0.4%]	−12.2%(−8.7%)[−0.9%]	−14.8%(−8.3%)[0.4%]	—(—)[0.4%]
Ca^{2+}	−5.3%(1.2%)[−0.4%]	−6.1%(0.8%)[−0.4%]	−10.6%(2.8%)[0.4%]	—(—)[0.0%]
Sn^{2+}	−9.9%(−4.2%)[−0.4%]	−11.1%(−4.6%)[−0.4%]	−14.9%(−3.1%)[0.4%]	—(—)[0.4%]
Sr^{2+}	−4.5%(2.3%)[−0.4%]	−4.9%(1.5%)[−0.8%]	−6.8%(3.8%)[0.4%]	—(—)[0.4%]
Ba^{2+}	−3.2%(3.9%)[−0.4%]	−3.9%(2.5%)[−0.4%]	−5.7%(6.0%)[0.4%]	—(—)[0.4%]
avg. value	−12.4%(−6.3%)[−0.4%]	−12.3%(−6.1%)[−0.6%]	−16.8%(−5.8%)[0.5%]	—(—)[0.5%]
SD	7.8%(7.3%)[0.2%]	7.6%(6.9%)[0.2%]	10.2%(8.2%)[0.1%]	—(—)[0.6%]

[a]The first values in the cells are for the HFE parameter set, the values in parentheses are for the CM parameter set while the ones in square brackets are for the IOD parameter set. Because of limited experimental values, only 16 M(II) cations are shown in the table.

curves and the NGC. After slightly tuning the parameters, the final LJ parameters can be determined. We employed Method 2 in this part, which is a more accurate way to obtain the HFE, IOD, and CM values. In the VDW-disappearing and VDW-appearing steps, we employed the soft-core scaling method instead of the linear or nonlinear scaling methods due to its better performance over the latter two.[53] In the present work, we also conducted tests among the different scaling methods and the data is given in Table 5. The L, K4, K6, and SC in Table 5 represent the linear scaling, nonlinear scaling with k = 4, nonlinear scaling with k = 6, and soft-core scaling methods, respectively, while all the windows involved a 300 ps simulation with the last 200 ps used to determine the free energy changes. It can be seen that the soft-core scaling method gives better-

converged and consistent results (i.e., the free energy of the VDW-appearing and VDW-disappearing processes have the opposite sign) than the other methods. The linear and nonlinear mixing methods could give consistent results for the small Be^{2+} ion but had more difficulty with larger ions such as Ba^{2+}.

The final parameters are shown in Table 6 (the HFE set), Table 7 (the IOD set), and Table 8 (the CM set), while the simulated HFE, IOD, and CN values corresponding to each set of parameters are provided in Tables 9a−9c. The HFE sets of parameters achieved a ± 1 kcal/mol accuracy, CM sets parameters all reached a ± 2 kcal/mol accuracy of relative hydration free energy while keeping the CN of most M(II) metal ions, the IOD sets of parameters obtained a good agreement with the experimental IOD values at the same time. Here, we treated the Zn^{2+} ion as an example again and showed the radial distribution functions for the different sets of parameters used in Figure 8. It could be seen that the CM parameter set yields a first solvation peak between those of the other two sets of parameters. Meanwhile, the IOD values and CNs are 1.67 Å with 4.1, 1.93 Å with 6.0, and 2.08 Å with 6.0 for the HFE, CM, and IOD sets of parameters, respectively.

Assessment of the Parameter Sets Developed in the Present Work. To further examine the reliability of the parameters determined in this work, in Table 10 we compared the $R_{min}/2$ values of the HFE set of parameters for the TIP3P water model with the VDW radii of metal ions[82] and LJ parameters for the monovalent ions determined in Joung and Cheatham's work.[22] The VDW radii of metal ions that have same electronic structures as noble gas atoms were calculated by Stokes employing the quantum mechanical scaling principle (QMSP)[82] while Joung and Cheatham designed the monovalent ions' LJ parameters specifically for PME Molecular Dynamics simulation by treating experimental HFEs as the primary target.[22] It can be seen that our parameters are quite close to the VDW radii obtained from the QMSP method while the M(II) metal ions all have smaller $R_{min}/2$ values than those of the monovalent cations in the same period, showing a good consistency between these sets.

Next, we analyzed the percentage errors with respect to the experimental HFE and IOD values for each of the parameter sets determined herein. These results are summarized in Tables 11a and 11b. From these data we can estimate the maximum error ranges. The values given in square brackets in Table 11a are for the IOD set, while the unbracketed values given in Table 11b are for the HFE set with the former indicating the maximum error in HFE (∼18% in TIP3P for Be^{2+}) if we get the IOD correct, while the latter is the maximum error we see in the IOD values (∼30% in TIP3P for Be^{2+}) if we get HFE correct. Hence, these values indicate the maximum error range associated with the modeling of M(II) cations using an unpolarized nonbonded model. Moreover, we observe the trend that the TIP3P, SPC/E, $TIP4P_{EW}$, and TIP4P water models have increasing errors successively. For all four water models, ions such as Be^{2+}, Cu^{2+} and Zn^{2+} have larger errors, presumably because of their strong coordination interaction with the surrounding waters. The alkaline-earth metal ions, except for Be^{2+}, have the smallest errors, likely because of their preference to form ionic bonds.

Build Your Own Parameters. The experimental HFEs of metal ions can be determined in different ways. In older works, most of the HFEs of ions were obtained from the NBS compilation on the basis of conventional values. In this situation, the HFE of the ions would change if the standard hydration free energy of a proton changes. Marcus treated $\Delta_{hyd}G^0[H^+] = -1056 \pm 6$ kJ/mol in his literature,[73] which comes from $\Delta_{hyd}H^0[H^+] = -1094$ kJ/mol, $\Delta_{hyd}S^0[H^+] = -131$ kJ/mol or $S_\infty[H^+(aq)] = -22.2$ J/K. However, various $\Delta_{hyd}G^0[H^+]$ values have been determined recently using different methods.[83−87] Tissandier et al. estimated the $\Delta_{hyd}G^0[H^+]$ value by employing the cluster-pair-based approximation,[86] while several other works concerning the computational estimation of the HFE of a proton have been published.[83−85] There are also experimental and theoretical efforts that predicted different HFEs from the targeted values used in this work for the same metal ions.[88,89] Regardless of the choices made, our data in the SI regarding the different combinations of LJ parameters for different water models would facilitate the design of parameter sets targeting data sets other than the one we used.[73]

CONCLUSIONS

First, we tested the transferability of LJ parameters determined in previous work and found that it was necessary to design new parameters for M(II) metal ions in PME simulations. Systematic studies were performed to determine the LJ parameters for M(II) metal cations using different water models with Lorentz−Berthelot combing rules in PME simulations. Hydration free energies, ion−oxygen distances in the first solvation peak as well as coordination numbers were determined for various combinations of LJ parameters by employing thermodynamics integration simulations employing the particle mesh Ewald summation method to model long-range electrostatics. The results showed there is a correlated relationship for the simulated HFE, IOD, and CN values. A series of curves were obtained using quadratic fitting procedures by treating the experimental values as targets based on the original data shown in SI. It was observed that different water models give different hydration free energies but highly similar structural properties when treating the same metal ions with identical parameters.

Generally, it is hard to reproduce all the experimental properties of the M(II) metal ions in aqueous solution using the nonbonded model due to its simplicity, which agrees with the former work of Ponomarev et al.[26] In general, the nonbonded model usually underestimates the interaction energy between metal ions and surrounding water molecules and is water model dependent. More interaction terms other than the LJ and Coulomb potentials should be considered in the force field in order to perform more accurate modeling of the M(II) metal ions. Meanwhile, polarized force fields[36−43] and short−long-range effective force (SLEF),[90] which consider short-range interactions such as polarization and charge transfer effects in more accurate ways, could also be promising methods to solve the dilemma of M(II) metal ion parameter design.

Through a consideration of the physical meaning of the VDW interaction, we fit a curve from experimental noble gas atom data to represent the relationship between the two parameters in the LJ potential. Along with the fitting curves obtained from scans of LJ grids, we arrived at three sets of parameters (HFE, IOD, and CM sets) for each of the TIP3P, SPC/E, and $TIP4P_{EW}$ water models employing a more detailed validation method. The HFE parameter sets used experimental HFEs as the target; the targeted property for the IOD sets is the experimental IOD values; while the CM parameters' aim is to reproduce the relative experimental HFEs and CNs. These

parameters accurately reproduced the target properties. We also investigated the underestimation of the HFE by the nonbonded model for different M(II) metal ions and found the errors are larger for the metal ions that could form stronger coordination interactions (i.e., covalent bonds) with surrounding waters. Finally, experimental values for the same M(II) metal ions may be variable due to different assumptions and standards employed; however, our data presented in the SI allows for the straightforward design of LJ parameters for M(II) metal ions, which could be helpful to those who want to target different experimental HFE, IOD, and CN values than used in our work.

■ ASSOCIATED CONTENT

Supporting Information

Details of the parameter fitting scheme, results from TI simulations, figures, and data sets for parametrized HFE, IOD, and CN values for various ion in different water models. This material is available free of charge via the Internet at http://pubs.acs.org.

■ AUTHOR INFORMATION

Corresponding Author

*Phone: 352-392-6973. Fax: 352-392-8722. E-mail: merz@qtp.ufl.edu.

Notes

The authors declare no competing financial interest.

■ ACKNOWLEDGMENTS

We thank Dr. Michael Weaver (UF) and Shuai Wang (UF) for many helpful discussions. We gratefully acknowledge financial support from the United States National Institutes of Health (RO1's GM044974 and GM066859) and computing support from the University of Florida High Performance Computing Center.

■ ABBREVIATIONS

HFE, hydration free energy; CN, coordination number; PME, particle mesh ewald; RDF, radial distribution function; LJ, Lennard-Jones; TI, thermodynamic integration; VDW, van der Waals; IOD, ion−oxygen distance

■ REFERENCES

(1) Tus, A.; Rakipović, A.; Peretin, G.; Tomić, S.; Šikić, M. *Nucleic Acids Res.* **2012**, *40*, W352−W357.
(2) Waldron, K. J.; Robinson, N. J. *Nat. Rev. Microbiol.* **2009**, *7*, 25−35.
(3) Rosenzweig, A. C. *Chem. Biol.* **2002**, *9*, 673−677.
(4) Thomson, A. J.; Gray, H. B. *Curr. Opin. Chem. Biol.* **1998**, *2*, 155−158.
(5) Peters, M. B.; Yang, Y.; Wang, B.; Füsti-Molnár, L. s.; Weaver, M. N.; Merz, K. M. *J. Chem. Theory Comput.* **2010**, *6*, 2935−2947.
(6) Dupureur, C. M. *Curr. Opin. Chem. Biol.* **2008**, *12*, 250−255.
(7) Andreini, C.; Bertini, I.; Cavallaro, G.; Holliday, G.; Thornton, J. *J. Biol. Inorg. Chem.* **2008**, *13*, 1205−1218.
(8) Chaturvedi, U. C.; Shrivastava, R. *FEMS Immunol. Med. Microbiol.* **2005**, *43*, 105−114.
(9) Berridge, M. J.; Bootman, M. D.; Lipp, P. *Nature* **1998**, *395*, 645−648.
(10) Christianson, D. W. *Prog. Biophys. Mol. Biol.* **1997**, *67*, 217−252.
(11) Lipscomb, W. N.; Sträter, N. *Chem. Rev.* **1996**, *96*, 2375−2434.
(12) Linder, M. C.; Hazegh-Azam, M. *Am. J. Clin. Nutr.* **1996**, *63*, 797S−811S.
(13) Holm, R. H.; Kennepohl, P.; Solomon, E. I. *Chem. Rev.* **1996**, *96*, 2239−2314.
(14) Coleman, J. E. *Annu. Rev. Biochem.* **1992**, *61*, 897−946.
(15) Berg, J. M. *Annu. Rev. Biophys. Biophys. Chem.* **1990**, *19*, 405−421.
(16) Chakravorty, D. K.; Wang, B.; Ucisik, M. N.; Merz, K. M. *J. Am. Chem. Soc.* **2011**, *133*, 19330−19333.
(17) Chakravorty, D. K.; Wang, B.; Lee, C. W.; Giedroc, D. P.; Merz, K. M. *J. Am. Chem. Soc.* **2011**, *134*, 3367−3376.
(18) Hoops, S. C.; Anderson, K. W.; Merz, K. M. *J. Am. Chem. Soc.* **1991**, *113*, 8262−8270.
(19) Chakravorty, D. K.; Parker, T. M.; Guerra, A. J.; Sherrill, C. D.; Giedroc, D. P.; Merz, K. M., Jr. *J. Am. Chem. Soc.* **2012**, *135*, 30−33.
(20) Lee, C. W.; Chakravorty, D. K.; Chang, F.-M. J.; Reyes-Caballero, H.; Ye, Y.; Merz, K. M., Jr.; Giedroc, D. P. *Biochemistry* **2012**, *51*, 2619−2629.
(21) Chakravorty, D.; Wang, B.; Lee, C.; Guerra, A.; Giedroc, D.; Merz, K., Jr. *J. Biomol. NMR* **2013**, 1−13.
(22) Joung, I. S.; Cheatham, T. E. *J. Phys. Chem. B* **2008**, *112*, 9020−9041.
(23) Babu, C. S.; Lim, C. *J. Phys. Chem. A* **2005**, *110*, 691−699.
(24) Pang, Y.-P. *Proteins: Struct., Funct., Bioinf.* **2001**, *45*, 183−189.
(25) Soniat, M.; Rick, S. W. *J. Chem. Phys.* **2012**, *137*, 044511−044519.
(26) Ponomarev, S. Y.; Click, T. H.; Kaminski, G. A. *J. Phys. Chem. B* **2011**, *115*, 10079−10085.
(27) Molina, J. J.; Lectez, S.; Tazi, S.; Salanne, M.; Dufreche, J.-F.; Roques, J.; Simoni, E.; Madden, P. A.; Turq, P. *J. Chem. Phys.* **2011**, *134*, 014511−014516.
(28) Chillemi, G.; D'Angelo, P.; Pavel, N. V.; Sanna, N.; Barone, V. *J. Am. Chem. Soc.* **2002**, *124*, 1968−1976.
(29) D'Angelo, P.; Barone, V.; Chillemi, G.; Sanna, N.; Meyer-Klaucke, W.; Pavel, N. V. *J. Am. Chem. Soc.* **2002**, *124*, 1958−1967.
(30) D'Angelo, P.; Zitolo, A.; Migliorati, V.; Chillemi, G.; Duvail, M.; Vitorge, P.; Abadie, S.; Spezia, R. *Inorg. Chem.* **2011**, *50*, 4572−4579.
(31) Mancini, G.; Sanna, N.; Barone, V.; Migliorati, V.; D'Angelo, P.; Chillemi, G. *J. Phys. Chem. B* **2008**, *112*, 4694−4702.
(32) Migliorati, V.; Chillemi, G.; D'Angelo, P. *Inorg. Chem.* **2011**, *50*, 8509−8515.
(33) Migliorati, V.; Mancini, G.; Chillemi, G.; Zitolo, A.; D'Angelo, P. *J. Phys. Chem. A* **2011**, *115*, 4798−4803.
(34) Beuchat, C.; Hagberg, D.; Spezia, R.; Gagliardi, L. *J. Phys. Chem. B* **2010**, *114*, 15590−15597.
(35) Tazi, S.; Molina, J. J.; Rotenberg, B.; Turq, P.; Vuilleumier, R.; Salanne, M. *J. Chem. Phys.* **2012**, *136*, 114507−114512.
(36) Piquemal, J.-P.; Perera, L.; Cisneros, G. A.; Ren, P.; Pedersen, L. G.; Darden, T. A. *J. Chem. Phys.* **2006**, *125*, 054511−054517.
(37) Grossfield, A.; Ren, P.; Ponder, J. W. *J. Am. Chem. Soc.* **2003**, *125*, 15671−15682.
(38) Jiao, D.; King, C.; Grossfield, A.; Darden, T. A.; Ren, P. *J. Phys. Chem. B* **2006**, *110*, 18553−18559.
(39) Dang, L. X. *J. Chem. Phys.* **1992**, *96*, 6970−6977.
(40) Dang, L. X.; Garrett, B. C. *J. Chem. Phys.* **1993**, *99*, 2972−2977.
(41) Smith, D. E.; Dang, L. X. *J. Chem. Phys.* **1994**, *100*, 3757−3766.
(42) Yu, H.; Whitfield, T. W.; Harder, E.; Lamoureux, G.; Vorobyov, I.; Anisimov, V. M.; MacKerell, A. D.; Roux, B. t. *J. Chem. Theory Comput.* **2010**, *6*, 774−786.
(43) Sakharov, D. V.; Lim, C. *J. Am. Chem. Soc.* **2005**, *127*, 4921−4929.
(44) Aaqvist, J. *J. Phys. Chem.* **1990**, *94*, 8021−8024.
(45) Merz, K. M. *J. Am. Chem. Soc.* **1991**, *113*, 406−411.
(46) Stote, R. H.; Karplus, M. *Proteins: Struct., Funct., Bioinf.* **1995**, *23*, 12−31.
(47) Aaqvist, J. *J. Phys. Chem.* **1994**, *98*, 8253−8255.
(48) Marrone, T. J.; Merz, K. M. *J. Phys. Chem.* **1993**, *97*, 6524−6529.
(49) Marrone, T. J.; Merz, K. M. *J. Phys. Chem.* **1994**, *98*, 8256−8257.
(50) Fyta, M.; Netz, R. R. *J. Chem. Phys.* **2012**, *136*, 124103−124111.
(51) Allnér, O.; Nilsson, L.; Villa, A. *J. Chem. Theory Comput.* **2012**, *8*, 1493−1502.

(52) Beutler, T. C.; Mark, A. E.; van Schaik, R. C.; Gerber, P. R.; van Gunsteren, W. F. *Chem. Phys. Lett.* **1994**, *222*, 529−539.
(53) Steinbrecher, T.; Mobley, D. L.; Case, D. A. *J. Chem. Phys.* **2007**, *127*, 214108−214113.
(54) Kollman, P. *Chem. Rev.* **1993**, *93*, 2395−2417.
(55) Hummer, G.; Szabo, A. *J. Chem. Phys.* **1996**, *105*, 2004−2010.
(56) Mitchell, M. J.; McCammon, J. A. *J. Comput. Chem.* **1991**, *12*, 271−275.
(57) Simonson, T.; Carlsson, J.; Case, D. A. *J. Am. Chem. Soc.* **2004**, *126*, 4167−4180.
(58) Mezei, M. *J. Chem. Phys.* **1987**, *86*, 7084−7088.
(59) Straatsma, T. P.; Berendsen, H. J. C. *J. Chem. Phys.* **1988**, *89*, 5876−5886.
(60) Jorgensen, W. L.; Chandrasekhar, J.; Madura, J. D.; Impey, R. W.; Klein, M. L. *J. Chem. Phys.* **1983**, *79*, 926−935.
(61) Berendsen, H. J. C.; Grigera, J. R.; Straatsma, T. P. *J. Phys. Chem.* **1987**, *91*, 6269−6271.
(62) Horn, H. W.; Swope, W. C.; Pitera, J. W.; Madura, J. D.; Dick, T. J.; Hura, G. L.; Head-Gordon, T. *J. Chem. Phys.* **2004**, *120*, 9665−9678.
(63) Case, D. A.; Cheatham, T. E.; Darden, T.; Gohlke, H.; Luo, R.; Merz, K. M.; Onufriev, A.; Simmerling, C.; Wang, B.; Woods, R. J. *J. Comput. Chem.* **2005**, *26*, 1668−1688.
(64) Shirts, M. R.; Pitera, J. W.; Swope, W. C.; Pande, V. S. *J. Chem. Phys.* **2003**, *119*, 5740−5761.
(65) Stone, J. E.; Hardy, D. J.; Ufimtsev, I. S.; Schulten, K. *J. Mol. Graphics Modell.* **2010**, *29*, 116−125.
(66) Yang, J.; Wang, Y.; Chen, Y. *J. Comput. Phys.* **2007**, *221*, 799−804.
(67) Stone, J. E.; Phillips, J. C.; Freddolino, P. L.; Hardy, D. J.; Trabuco, L. G.; Schulten, K. *J. Comput. Chem.* **2007**, *28*, 2618−2640.
(68) Rodrigues, C. I.; Hardy, D. J.; Stone, J. E.; Schulten, K.; Hwu, W.-M. W. In *Proceedings of the 5th Conference on Computing Frontiers*; ACM: Ischia, Italy, 2008, p 273−282.
(69) Preis, T.; Virnau, P.; Paul, W.; Schneider, J. J. *J. Comput. Phys.* **2009**, *228*, 4468−4477.
(70) Liu, W.; Schmidt, B.; Voss, G.; Müller-Wittig, W. *Comput. Phys. Commun.* **2008**, *179*, 634−641.
(71) Liu, W.; Schmidt, B.; Voss, G.; Müller-Wittig, W. Molecular Dynamics Simulations on Commodity GPUs with CUDA. In *High Performance Computing*, 14th International Conference, Goa, India, Dec. 18−21, 2007; Aluru, S., Parashar, M., Badrinath, R., Prasanna, V., Eds.; Springer: Berlin/Heidelberg: 2007; Vol. *4873*, pp 185−196.
(72) Friedrichs, M. S.; Eastman, P.; Vaidyanathan, V.; Houston, M.; Legrand, S.; Beberg, A. L.; Ensign, D. L.; Bruns, C. M.; Pande, V. S. *J. Comput. Chem.* **2009**, *30*, 864−872.
(73) Marcus, Y. *J. Chem. Soc., Faraday Trans.* **1991**, *87*, 2995−2999.
(74) Marcus, Y. *Chem. Rev.* **1988**, *88*, 1475−1498.
(75) Miyanaga, T.; Watanabe, I.; Ikeda, S. *Chem. Lett.* **1988**, *17*, 1073−1076.
(76) Ohtaki, H.; Radnai, T. *Chem. Rev.* **1993**, *93*, 1157−1204.
(77) Jalilehvand, F.; Spångberg, D.; Lindqvist-Reis, P.; Hermansson, K.; Persson, I.; Sandström, M. *J. Am. Chem. Soc.* **2000**, *123*, 431−441.
(78) Smirnov, P. R.; Trostin, V. N. *Russ. J. Gen. Chem.* **2011**, *81*, 282−289.
(79) Netz, R. R.; Horinek, D. *Annu. Rev. Phys. Chem.* **2012**, *63*, 401−418.
(80) Jones, J. E. *Proc. R. Soc. London, A* **1924**, *106*, 463−477.
(81) Radëtìsig, A.; Smirnov, B. *Reference Data on Atoms, Molecules, and Ions*; Springer-Verlag: Berlin and New York, 1985.
(82) Stokes, R. *J. Am. Chem. Soc.* **1964**, *86*, 979−982.
(83) Mejias, J. A.; Lago, S. *J. Chem. Phys.* **2000**, *113*, 7306−7316.
(84) Tawa, G. J.; Topol, I. A.; Burt, S. K.; Caldwell, R. A.; Rashin, A. A. *J. Chem. Phys.* **1998**, *109*, 4852−4863.
(85) Topol, I. A.; Tawa, G. J.; Burt, S. K.; Rashin, A. A. *J. Chem. Phys.* **1999**, *111*, 10998−11014.
(86) Tissandier, M. D.; Cowen, K. A.; Feng, W. Y.; Gundlach, E.; Cohen, M. H.; Earhart, A. D.; Coe, J. V.; Tuttle, T. R. *J. Phys. Chem. A* **1998**, *102*, 7787−7794.
(87) Zhan, C.-G.; Dixon, D. A. *J. Phys. Chem. A* **2001**, *105*, 11534−11540.
(88) Schmid, R.; Miah, A. M.; Sapunov, V. N. *Phys. Chem. Chem. Phys.* **2000**, *2*, 97−102.
(89) Asthagiri, D.; Pratt, L. R.; Paulaitis, M. E.; Rempe, S. B. *J. Am. Chem. Soc.* **2004**, *126*, 1285−1289.
(90) Wu, R.; Lu, Z.; Cao, Z.; Zhang, Y. *J. Chem. Theory Comput.* **2011**, *7*, 433−443.

NOTE ADDED AFTER ASAP PUBLICATION

This article was published ASAP on May 23, 2013, with a corrupted Supporting Information file. The corrected version was published on May 24, 2013.